Development of a Piezo-Capacitive Tactile Force Sensor for Measuring Static and Dynamic Forces in Minimally Invasive Robotic Surgeries.

By

Maira Ehsan Mughal

(Registration Number 00000363399)

Supervised by

Dr. Hamid Jabbar

Department of Mechatronics Engineering

College of Electrical & Mechanical Engineering

National University of Sciences & Technology (NUST)

Islamabad, Pakistan

(2024)

THESIS ACCEPTANCE CERTIFICATE

Certified that final copy of MS/MPhil thesis by Ms. Maira Ehsan Mughal Registration No.363399, of Electrical and Mechanical Engineering College has been vetted by undersigned, found complete in all respects as per NUST Statues/Regulations, is free of plagiarism, errors, and mistakes and is accepted as partial fulfillment for award of MS/MPhil degree. It is further certified that necessary amendments as pointed out by GEC members of the scholar have also been incorporated in the said thesis.

Signature: _____

Name of Supervisor: Dr. Hamid Jabbar

Dated: 15 Aug 2024

Signature of HOD: _____

Dr. Hamid Jabbar

Date: 15 Aug 2024

Signature of Dean: _____

Brig Dr. Nasir Rashid

Date: 15 AUG 2024

DEDICATION

I would like to dedicate this work to my parents, whose unwavering support and sacrifices have been my greatest motivation.

ACKNOLEDGEMENTS

First and foremost, I am profoundly thankful to my Creator, Allah Subhanahu Wa Ta'ala, for His divine guidance and blessings throughout this journey. Without His mercy and wisdom, this work would not have been possible.

I extend my deepest gratitude to my beloved parents for their unconditional love, unwavering support, and understanding. Their sacrifices and prayers have been the backbone of my achievements. I am equally thankful to my sisters, Nabeeha and Maham, for their endless love and encouragement, which have been a constant source of strength for me.

I would also like to express my heartfelt acknowledgement to my supervisors, Dr. Hamid Jabbar and Dr. Mubashir Saleem, for their invaluable guidance and mentorship. Their commitment to excellence has inspired me to strive for betterment in every aspect of my work.

I am grateful to my GEC members, Dr. Hassan Elahi and Dr. Mohsin Islam Tiwana, for their insightful analysis and assessment of my research. Their constructive feedback has played a crucial role in refining my work.

A special thanks goes to my seniors, Muhammad Rehan and Usman Khan, for their continuous support and for always being available to guide me. Their experience and support have been instrumental in helping me navigate through challenges.

Lastly, I am deeply thankful to my dear friends, Qurat-ul-Ain, Shoaib, Harris, and Uzair, for their unwavering companionship. Their encouragement and positive energy have kept my motivation intact throughout this journey.

ABSTRACT

Taking inspiration from the human tactile system, this paper presents a sensitive biomimetic multimodal tactile sensor designed for the discrimination of static and dynamic forces. The multimodal tactile sensor integrates a piezoelectric-capacitive tandem mechanism to respond to dynamic and static forces, respectively. The sensor is capable of detecting normal direction dynamic force signals using a piezoelectric component operating in the d33 mode, while static force detection is achieved through a capacitive component.

The capacitive sensing part features a unique configuration with a top electrode and two sets of differential pairs of electrodes for force measurement in the X and Y shear axes, along with a single electrode for normal force measurement. This innovative design allows for precise force measurements across multiple directions. Experimental characterization of the sensor was conducted for static, quasi-static, and dynamic forces, demonstrating its capability to respond to dynamic forces up to 60Hz.

The force sensitivity of the sensor for normal forces is measured at 0.084 pF/N for the capacitive part and 0.035 V/N for the piezoelectric part, within a force range of 10N. In the shear X and Y directions, the sensor exhibited sensitivities of 0.027 pF/N and 0.029 pF/N, respectively, within a force range of 1.2N. These results highlight the sensor's high sensitivity and accuracy in force measurement.

Given its dimensions, performance, and capabilities, the presented sensor holds significant potential for applications in minimally invasive robotic surgeries, robotics, wearable devices, and prosthetics. Its ability to accurately measure both static and dynamic forces makes it a valuable tool for enhancing tactile feedback and control in various advanced technological applications. This sensor represents a substantial advancement in the development of biomimetic tactile sensing devices, paving the way for more sophisticated and responsive systems in both medical and non-medical fields.

Key Words: *Tactile sensor, Multi-axis Force Sensor, capacitive-piezoelectric, Multimodal force sensor, Biomimetic Tactile Sensor, minimally invasive Robotic Surgeries (MIRS), Mechanoreception, Force sensing, Dynamic force detection, Static force detection, Shear force measurement, Sensor characterization, Biomedical applications, Wearable technology, Robotic prosthetics, Sensor integration, Smart sensors, Disposable sensors*.

Contents

List of Figures

List of Tables

Chapter 1: INTRODUCTION

In many natural systems, the sense of touch, also known as tactile sensing, is critical for manipulative and exploratory tasks. In humans, even a temporary loss of touch in the fingers due to cold makes a simple task like buttoning a shirt difficult. Tactile sensing, in general, uses physical contact to provide information about shape, temperature, texture, shear and normal forces, pressure, and vibrations. Despite the importance of tactile sensing in nature, it is not present in current robotic systems. Tactile feedback would allow dexterous manipulation of objects as well as detection of textures and other physical stimuli in humanoid robots and prosthetics [1]. Tactile feedback via medical instruments could also be used in minimally invasive surgery (MIS) to detect anatomical changes caused by diseases, such as tumors, kidney stones, and arterial stenosis [2].

Robot-assisted surgeries have gained a lot more importance in previous years. There are many surgical robots that are commercially available and that can perform the procedures such as laparoscopic surgeries, ocular surgeries and cancerous tissue removal. Whereas the major limitation of these robotic surgical systems is the loss of tactile force feedback during the surgical procedure, which can cause damage to tissue or organ during the procedure and there is a chance of trauma and blood loss. To improve the efficiency of the surgical robotic systems there is a dire need for a force feedback system for robot-assisted surgeries and minimally invasive robotic surgeries (MIRS). This chapter focuses on the benefits and limitations of minimally invasive robotic surgeries, types of tactile feedback and different application of tactile force sensors with surgical tools and systems.

1.1 Aim and Objectives

A detailed literature review which is summarized in Chapter 2, shows that there have been many attempts in recent times to restore tactile force feedback in MIS and MIRS, but many have not yielded clinically acceptable results due to their own limitations. In the literature review first the single transduction mechanism based tactile sensors have been discussed in detail along with the pros and cons each transduction has to pose, and then there is a detailed overview of the Multi transduction tactile sensors and how they are bridging the gaps created by the single transduction mechanism. Also there has been a progression in bringing tactile sensing technology closer to the human sensing system, so biomimetic tactile sensing solutions are getting research interests these days; so around multi-modality and biomimicry the objective of this thesis revolves. The motivations behind this research are:

1. As the progression in tactile sensing and its integration in MIRS, is focused towards developing ***sensing system comparable to human tactile sensing*** capabilities, so this force sensor will be a step forward towards reaching this goal.
2. The **maneuvering of the deep-seated tissues** can be possible with greater accuracy (transduction mechanism fusion) and in a ***larger bandwidth***.
3. As the sensor is mimicking human tactile system, so it can be a Minimally Invasive alternative to surgeon's hand for manual ***tissue palpations*** for removing the cancerous cells from the healthy cells.

the objectives of this research are:

1. Design of tactile sensor with the hybrid transduction mechanism (Piezoelectric + Capacitive).
2. Fabricated sensor should have an ability to respond to static and dynamic signals in the frequency range 0-50Hz.
3. Fabricated sensor should be dimensionally compliant with MIS procedures.
4. Fabrication and experimental characterization of the sensor.

1.2 Minimally Invasive Robotic Surgery (MIRS)

Robots have gained a lot of importance in the medical field and surgical procedures. MIS is a procedure in which a surgeon uses small skin incisions to access the internal anatomy of the human body to perform any operation and when a robot assists in this procedure it is referred to as minimally invasive robotic surgery (MIRS). By using the MIRS technique, the anesthesia time for operation, loss of blood during the procedures and trauma is reduced and the overall recovery time of the patient is also minimized. The commercially available MIRS systems include the ZEUS^{TM} and the da Vinci^{TM} robotic surgical systems [3], [4]. As shown in Figure 1.1 the robotic surgical systems have master-slave consoles, the master console is for the surgeon to operate the tools and the slave console is at the patient side for procedures using tools. MIRS has many benefits for the surgeon also because it requires less effort and the output of the surgery or procedure is also up to the marks. The limitation of these robotic surgical systems is that the surgeon is unable to get an idea of how much grasping force is being exerted during tissue manipulation or any other procedure because the skin incision is very small and this may cause extensive force application and may damage organs as well. In conventional surgery methods, the sense of touch plays an important role and to achieve this in MIS and MIRS the utilization of flexible tactile sensors for medical surgery and robotic manipulations has made it possible [5], [6]. da Vinci^{TM} surgical robot is the first and most successful commercially available surgical robot also doesn't provide force feedback or tactile feedback and it has also been reported that by using force feedback during the grasping applications using the da Vinci^{TM} robot the grasping force can be reduced [7]. The estimation of tool tissue interaction forces during the MIRS is still a challenge and requires a new method to acquire force feedback [8].The worst thing that can happen during surgery is causing harm during the procedure. The opposing argument is that avoiding harm is the most important thing. As arteries are hidden in some tissues and cutting them can be critical therefore there is a high risk of causing harm to arteries during the procedures of MIS and MIRS. This risk is minimal in open surgery because the surgeon can inspect by hand and sense the hidden arteries. A pressurized vessel can always be detected by feeling a light pulse within tissues with the fingertip. Thus, a surgeon will palpate any unknown tissue before performing a blunt dissection to avoid uncontrolled bleeding risk and trauma [1], [2]. This is impossible in MIS because there is no close exposure with the tissue under the procedure, and even more so in MIRS because the patient and surgeon are separated mechanically. There is always the possibility of damaging an artery. Unintended bleeding in MIS and MIRS is also an issue and stopping it takes longer because it is more time-consuming than open surgery. Blood can also contaminate the endoscope, potentially causing complete blindness and forcing the surgeon to switch to open surgery during the procedure, causing time delays and possibly putting the patient's life in danger. The problem's relevance is demonstrated by the following three examples:

- A known, serious complication of laparoscopic hernioplasty (inguinal hernia repair) using MIS is laceration of the epigastric arteries, which can result in severe bleeding [9–11]. Because the iliac and femoral vessels are specifically affected [11], the patient may lose a leg. This is especially important because inguinal hernia surgery is one of the most common procedures, at least in Germany and the United States [12].
- Another frequently performed procedure is cholecystectomy (gall bladder removal). More than 80% of procedures in modern health care are minimally invasive [13]. Due to anatomical variations, bleeding of the cystic and/or proper hepatic arteries, as well as lesions of vascular structures within the hepato-duodenal ligament, are common complications. In this case, complications may increase and an MIS may be required to be converted to open surgery.
- In minimally invasive surgery, there is currently no method for locating invisible arteries. Their forces are too low for force feedback detection, and the covering tissue prevents optical discovery. This is not only inconvenient for the surgeon, but it also poses a serious risk to the patient due to the possibility of damaging a hidden artery. Even in standard procedures, a possible check for hidden arteries before any dissection can improve patient safety and surgery quality [14].

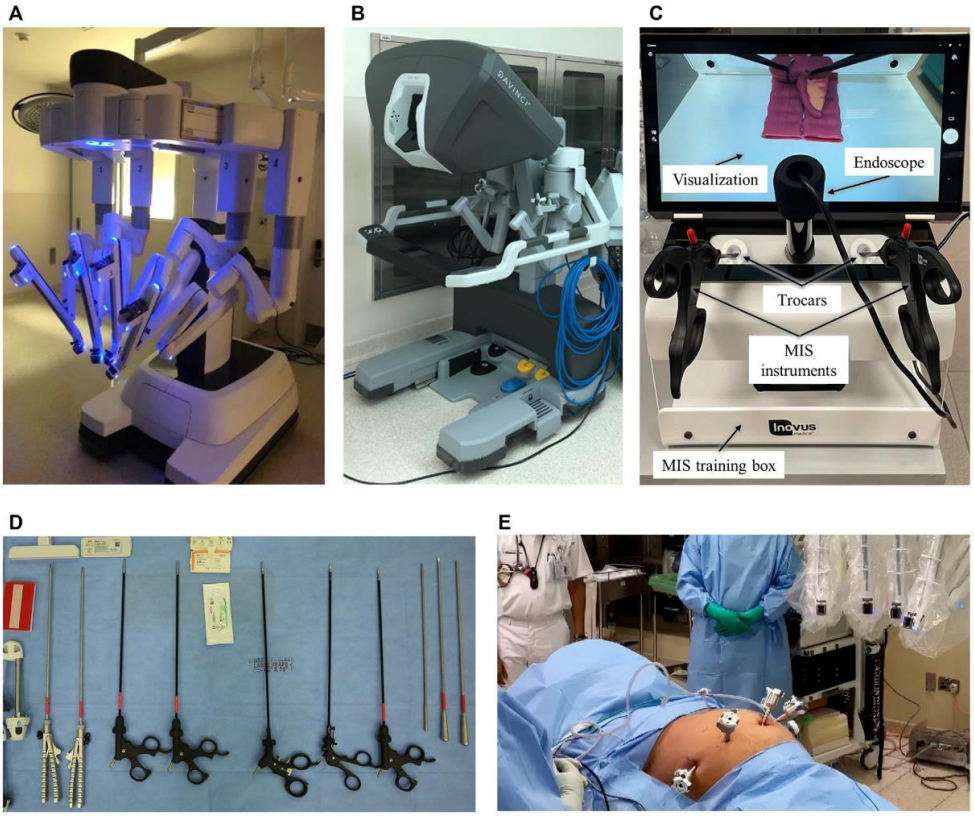

Figure 1.1 Minimally Invasive Surgery Systems. (A,B) Da Vinci surgical robotic system for MIS: (A) patient cart holding the camera and instruments that the surgeon controls remotely and (B) surgeon console that controls the instrumented arms and provides a high-definition 3D view of the operation site. (C) Laparoscopic box trainer with an endoscope and surgical instruments used for MIS simulations. (D) Surgical instruments used in laparoscopic surgery and training. (E) Laparoscopic operation with port accesses in the abdominal cavity and the docking of the robot arm with the ports [14].

1.3 Tactile sensors and their types

A tactile sensor is a device that can measure quantity or property upon physical contact with any object. Some definitions say that a tactile sensor can only measure force but it is not limited to force, any quantity which can be detected upon physical contact using a sensor can be referred to as a tactile sensor. The shape of the object, the texture of the object, temperature, moisture and pressure can also be some physical quantities that can be measured using tactile sensors [15]. This study focuses on the design, fabrication and experimental characterization of a tactile force sensor for robotic surgical systems [16].

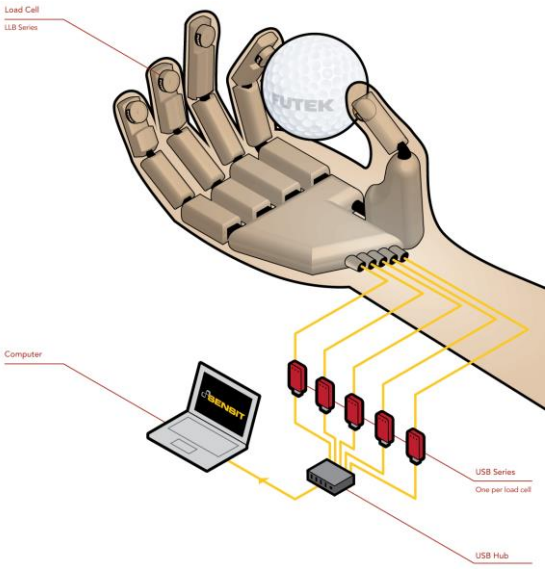

Figure 1.2 A wearable tactile sensor for object grasping feedback [16]

1.4 Characteristics of a Tactile Sensor considering Robotic Surgical System

Keeping in view the robotic surgical systems the tactile sensor designed for this application would be desirable if it had the following attributes:

1. The size of the tactile sensor must be compliant with surgical tools.
2. The sensor must be able to detect and decouple force components in 3D space, meaning that the sensor is sensitive to both the normal and shear force components.
3. The sensor must be sensitive to dynamic forces because in robotic surgeries there can be any type of input force whether it can be static or dynamic.
4. Moreover, low hysteresis and better repeatability are also some concerns when designing tactile sensors for surgical robotic systems and tools.
5. The tactile sensor which is being used in the robotic surgical system must be of biocompatible material.
6. It will be better if it is disposable.

1.5 Application of Tactile Force Sensors in Robotic Surgical Systems

The tactile force sensors can be used in endoscopic probes and surgical palpation probes which can be used for tumor stiffness detection and cancerous tissue removal as a result a better idea of contact force can be acquired. In laparoscopic surgeries, tactile sensors can be mounted on surgical grippers and forceps for the assessment of the applied force and direction of force when surgery is being performed. During the ocular massage in anesthesia training models, the tactile force sensor can be used to measure the applied force and direction also for needle block device where force applications are required in a gentle way [17].

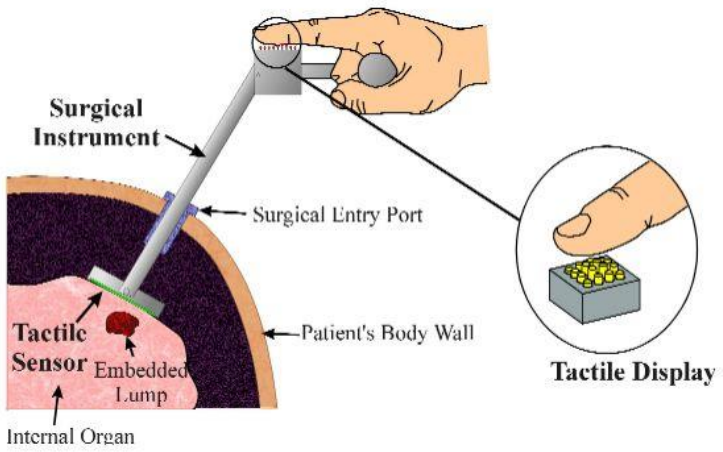

Figure 1.3 A remote palpation probe with integrated tactile force sensor at the jaws of gripper [17]

Chapter 2: Literature Review

Many different types of tactile sensors exist based on their working principle and transduction mechanisms, for example capacitive. piezoresistive, piezoelectric, inductive, magnetic, and optical. This chapter contains a review of the different tactile force sensors based on the different transduction mechanisms. Moreover, the pros and cons of different transduction mechanisms are also discussed in this chapter.

2.1 Tactile Force Sensors based on Different Transduction Mechanisms

In the literature, tactile force sensors are based on multiple kinds of transduction mechanisms. Based on the design and working principle these tactile sensors can sense forces in single axis and multi axis. The sensing element which is also known as force transfer medium is usually a soft and deformable material so that it can deform to transfer force to the structure used for sensing. In the literature, the sensing element is usually made up of soft materials such as plastics [18], yarns/fabrics [19], and silicone elastomers [20]. These soft materials must be biocompatible keeping in view the robotic surgery so that it should not disturb or damage any body organ. Some of the tactile force sensors based on different transduction mechanisms are discussed below.

2.1.1 Capacitive Tactile Force Sensors

Capacitive sensors use the change in the overlap area of capacitive plates and the change in the gap between the plates to detect the capacitance change depicting shear and normal forces. Zhang et al. 2020 [21] proposed a capacitive tactile sensor (CTS). Stoppers are designed to deter structural deformation when normal forces are applied to realize a high detection sensitivity and wide dynamic range. The sensor provides operation flexibility in normal force detections and unaltered supportiveness on shear force and its angle detections. Different techniques such as higher dielectric materials and needle-like structures are used to increase the sensitivity of capacitive sensors. Liu et al. 2021 [22] presented a flexible 3D tactile sensor using crossbar walls and micropillar arrays as a dielectric with optimized Young's Modulus. The crossbar structure ensures a fixed overlap area.

2.1.2 Piezoelectric Tactile Force Sensors

Piezoelectric sensors use the phenomenon that when stress is applied electric potential is generated across the body. Sokhanvar et al. [23] proposed a MEMS-based piezoelectric sensor for MIS which was utilized for endoscopic instruments. They utilized MEMS-based fabrication technology for PVDF films and MIS graspers mounting. In a similar study for detecting submucosal tumors in endoscopic procedures, Chuang et al. [24] fabricated a tactile sensor based on piezoelectric transduction modality. The sensor was enclosed in soft layers of polydimethylsiloxane (PDMS) and copper ball, PVDF was used as a piezoelectric element. The sensor was incorporated with an endoscopic probe to detect hidden tumors in healthy tissues.

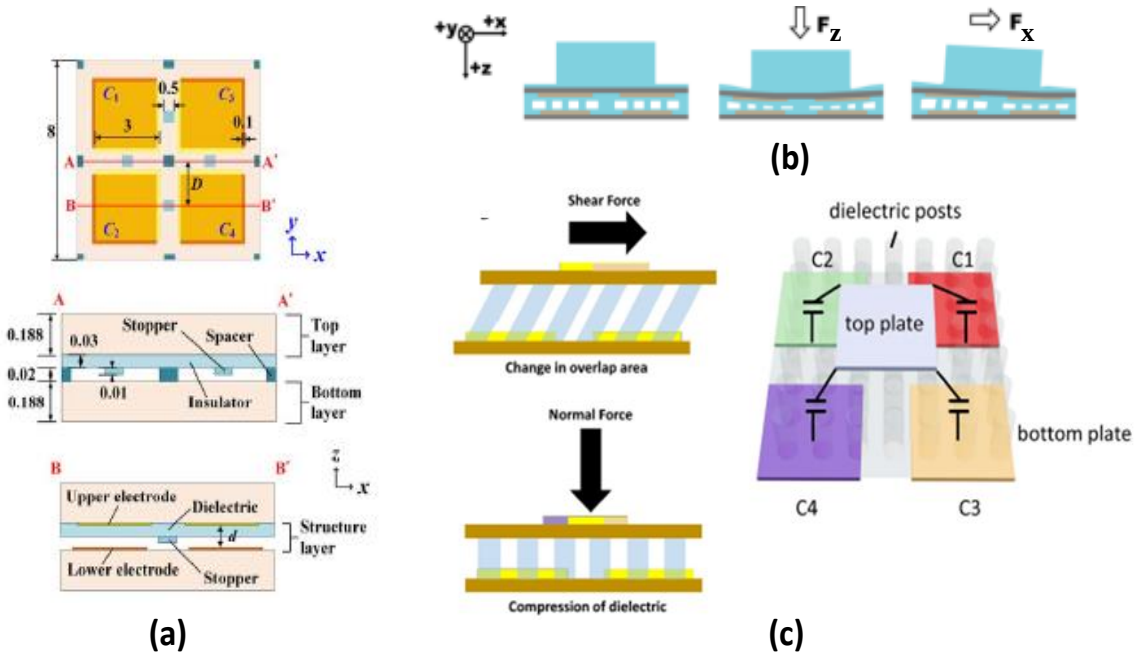

Figure 2.1 (a) Schematics of a capacitive tactile force sensor [21] (b) Working principle of capacitive tactile force sensor (c) Design of a capacitive tactile force sensor with single top electrode [22]

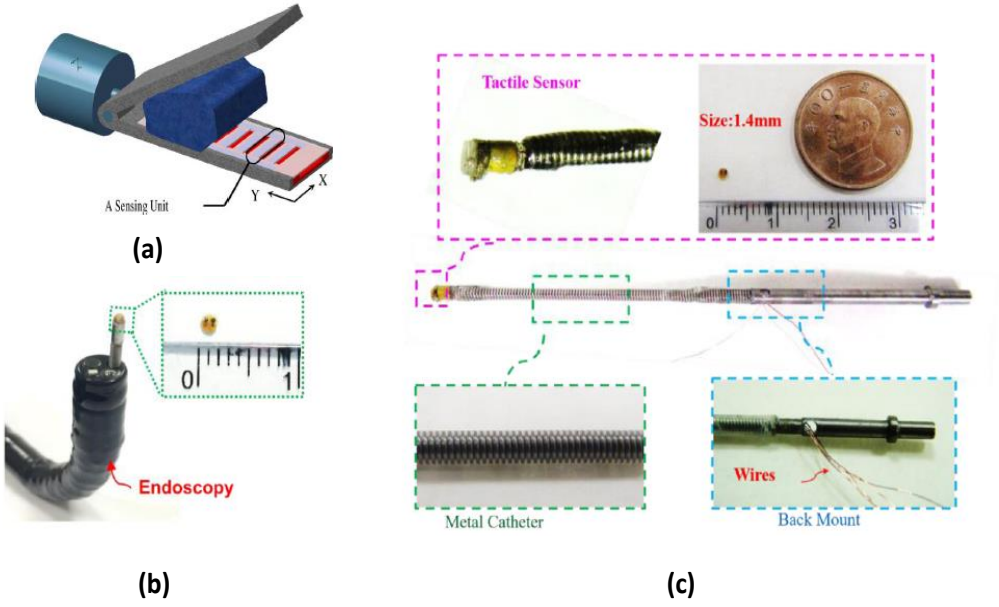

Figure 2.2 a) PVDF films mounted on a gripper acting as piezoelectric tactile force sensor [23] (b) MEMS based piezoelectric tactile force sensor mounted on endoscopic probe [24] (c) Piezo electric tactile force sensor mounted on catheter tip [24]

2.1.3 Piezoresistive Tactile Force Sensor

Piezoresistive sensors use strain gauges [25], [26]. Dargahi and Najarian [13] proposed sensorized graspers with micro strain gauges mounted on the forceps, an electronic feedback system was also developed to analyze the applied force on the LED bar graph. Tanimoto et al. [27] presented a sensor system for intra-vascular neural surgery using micro piezoresistive strain gauges, the sensor was able to measure the interaction force between the catheter and blood vessels. Piezoresistive strain gauges were placed on a silicon diaphragm for sensing, and they tested their sensor on the canine model of an animal. In another effort King et al. [28] Used Flexi Force™ piezoresistive strain gauges on a tool of the da Vinci™ surgical robotic system, they were able to measure grasping forces. Their study explained that the feedback of force in robotic surgery can enhance safety by reducing the gripping forces during the surgical procedures.

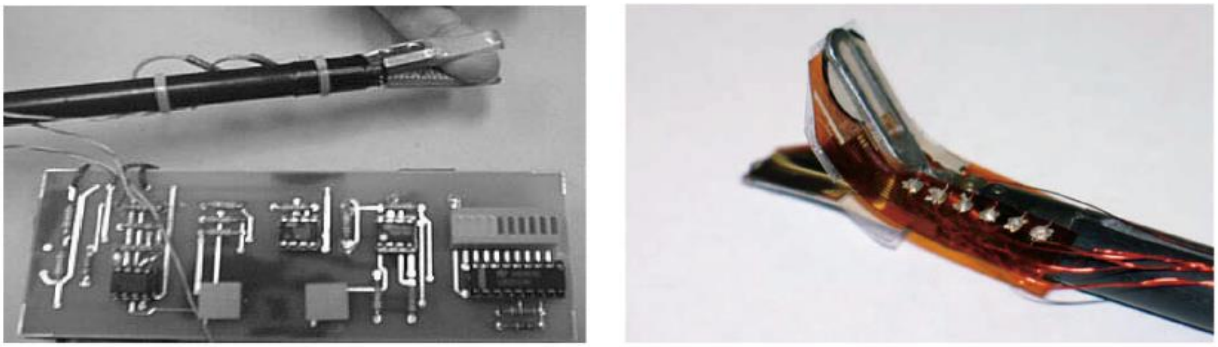

Figure 2.3 Micro strain gauges mounted at grippers with a feedback system for estimating input force [27] (b) Flexi force sensors mounted on forceps of daVinci surgical robot [28].

2.1.4 Inductive Tactile Force Sensors

Inductive tactile sensors work on the principle of inductance change due to ferromagnetic marker movement embedded in the elastomer. Kawasetsu et. al. [29] proposed a tactile sensor based on the inductive principle, four round coils were placed on flexible PCB and a soft ferromagnetic marker was embedded in an elastomer. Although no specific application in robotic surgery was not discussed but the sensor was able to measure forces in Normal and shear directions. In another study, Hongbo et. al. [30] presented a similar inductive tactile force sensor but the working principle was a little bit different the inductive coils were the same as proposed by Kawasetsu et. al. [29] but instead of a ferromagnetic marker they used aluminum sheet. The working topology was based on the eddy current effect. The proposed sensor was able to mount on surfaces of grippers because of its small size and flexible PCB layer. It was able to sense both normal and shear forces.

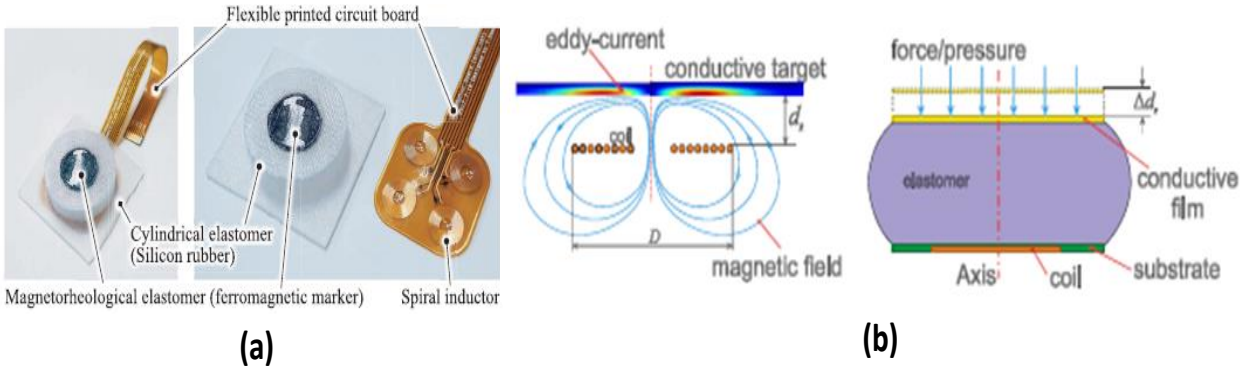

Figure 2.4 (a) A tri-axis inductive tactile force sensor [29] (b) Working principle of eddy current effect based inductive tactile sensor [30]

2.1.5 Optical Tactile Force Sensor

Song et. al. [31] presented a novel 3D high-density tactile sensor based on an optical transduction mechanism. The design was inspired by the human eye and can detect normal and shear forces with the sensitivity of 0.000280 mN/Gray and 0.0262 N/µm respectively. The sensor was designed keeping in view the surgical applications and robotic manipulations. Massaro et. al. [32] proposed a MEMS-based optical tactile sensor which worked on the principle of fiber optics. Tasks like roughness detection and shape recognition were also performed by integrating this sensor on a robotic finger.

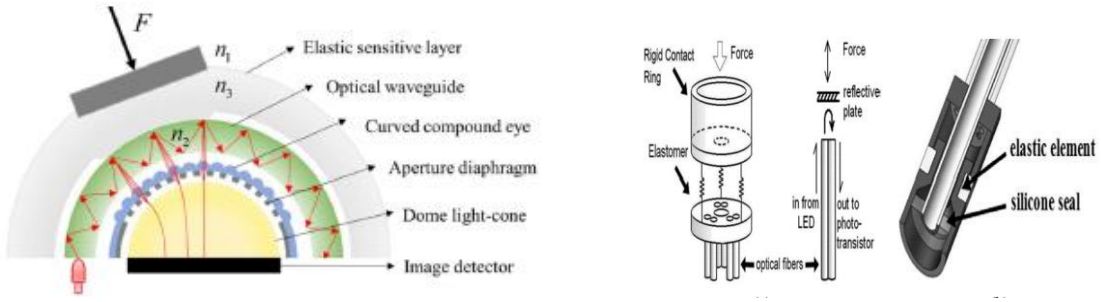

Figure 2.5 (a) Optical tactile force sensor based on bionic eye compound [31] (b) A fiber optic-based MEMS force tactile sensor [32]

2.1.6 Magnetic Tactile Force Sensor

Many magnetic field based tactile force sensors were presented in the literature with different designs and enhanced sensing capabilities. In 2014 Youssefian et. al. [35] proposed a tactile sensor for achieving force feedback during gripping and grasping robotic applications using Hall sensors. The sensor was able to detect tri-axial forces only at very low force ranges like 1.2 N for normal and 0.2 N for shear forces. Chathuranga et. al. [36] proposed a disposable force sensor for biomedical applications and MIS. The sensor was based on three hall effect sensors placed orthogonally. The magnet was embedded in a soft elastomer so that the sensing range was improved. The displacements were modelled analytically using mathematical formulations. The sensor was able to detect normal and shear forces. Jamone et. al. [37]

presented a sensor for the fingers of a robot, they used a single axis hall effect sensor, and the magnet was embedded in the elastomer.

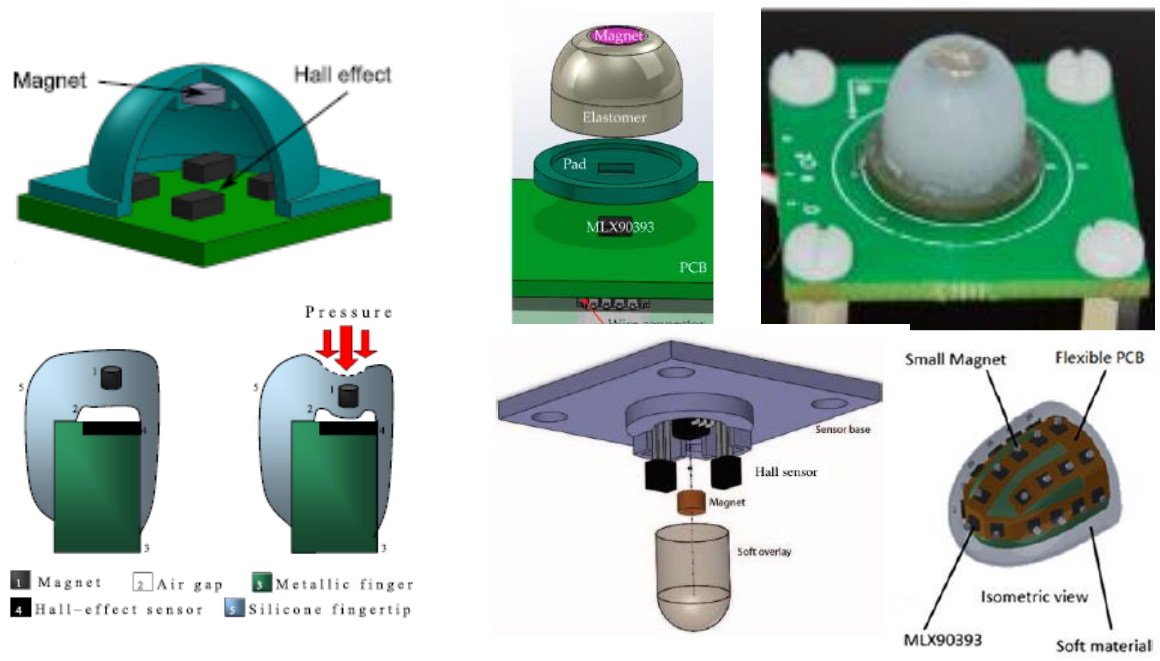

Figure 2.6 Tactile force sensors working on magnetic transduction principle presented in the literature based on single-axis and tri-axis Hall sensors [35][37][39]

2.2 Comparison of Transduction Mechanisms for Tactile Force Sensing

Table 2.1 contains a comparison summary of tactile sensors based on different transduction mechanisms for robotic surgery, although the tactile force sensors proposed in the literature are small in size, made up of soft materials and able to detect normal and shear forces but the main disadvantages of proposed sensors in literature are hysteresis, nonlinearity, inconsistency in the output readings and expensive fabrication. As compared to other transduction mechanisms, tactile forces sensors which are based on the magnetic transduction principle have many advantages of excellent linearity, better repeatability, low hysteresis, low-cost fabrication, and robustness [1], [47].

Table 2.1 Different transduction mechanisms and their comparison [12,47,48]

Transduction Mechanisms	Advantages	Disadvantages
Capacitive	Excellent sensitivity, High resolution, High dynamic range, No temperature effects	Stray capacitances, Complex readout electronics, Noise dependency, Large Hysteresis, Non-Linearity
Piezoresistive	Simple fabrication, High spatial resolution, Cost-effective, VLSI compatible	Hysteresis errors, High power consumption, Lack of repeatability, Poor Reliability
Piezoelectric	Excellent frequency response, better accuracy, High sensitivity, Large dynamic range	Poor spatial resolution, Charge leakages, Poor response toward static forces
Optical	Better reliability, large sensing range, High repeatability	Bulky size, Output dependent on temperature or misalignment
Magnetic/Inductive	High linearity, High sensitivity, Large dynamic range, Low fabrication cost	High power consumption, Noise in output signals

2.3 Multi-modal Tactile Sensors:

Multimodal tactile sensors have emerged as a significant innovation in the field of tactile sensing technology. While individual transduction mechanisms like piezoelectric, capacitive, resistive, and optical sensors each offer unique advantages, they also come with inherent limitations. The integration of multiple sensing modalities within a single sensor addresses many of these limitations and offers enhanced performance, reliability, and versatility.

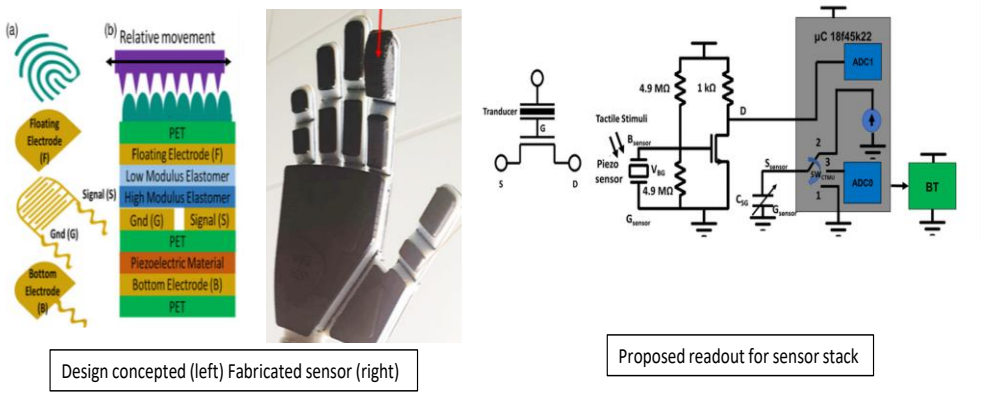

Figure 2.7 A multi-modal capacitive and piezoelectric tactile sensor and its proposed readout strategy [49]

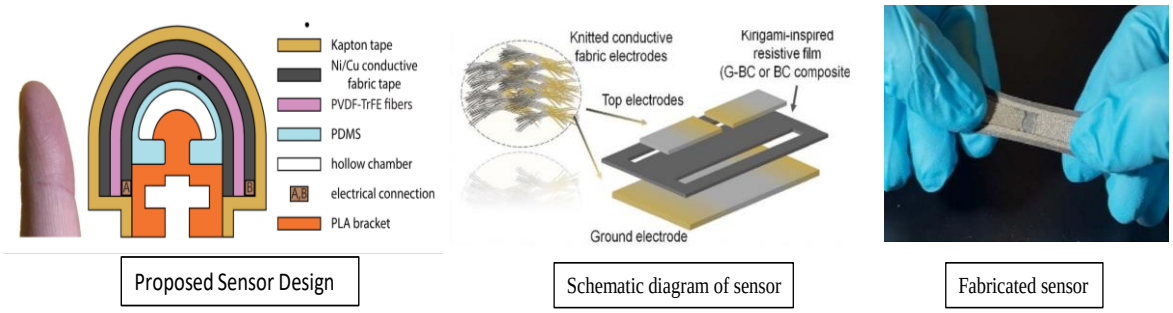

Figure 2.8 Multimodal piezoelectrical and capacitive sensor

2.3.1 Enhanced Sensory Information

One of the primary benefits of multimodal tactile sensors is the ability to gather a richer set of sensory data. Single-mode sensors are often limited in the type of information they can provide. For example, a capacitive sensor can detect pressure changes but may struggle with temperature variations. By combining capacitive sensing with thermosensitive elements, a multimodal sensor can concurrently measure both pressure and temperature, providing a more comprehensive understanding of the tactile environment.

2.3.2 Improved Accuracy and Precision

Multimodal tactile sensors can significantly enhance the accuracy and precision of measurements. By cross-referencing data from different sensing modalities, these sensors can reduce the likelihood of errors and improve the reliability of the collected data. For instance, in a robotic application, a multimodal sensor combining resistive and piezoelectric elements can better distinguish between different types of contact forces and textures. This synergy allows for more precise manipulation and interaction with objects, which is crucial for tasks requiring delicate handling.

2.3.3 Increased Robustness and Reliability

Reliability is a critical factor in the performance of tactile sensors, particularly in challenging environments. Multimodal tactile sensors benefit from the redundancy of having multiple sensing mechanisms. If one mode fails or is compromised due to environmental factors such as temperature fluctuations or electromagnetic interference, other modes can compensate, ensuring continuous and reliable operation. This robustness is particularly valuable in applications such as prosthetics, where consistent sensory feedback is essential for user confidence and functionality.

2.3.4 Versatility

The versatility of multimodal tactile sensors extends their applicability across various fields. In robotics, these sensors enable robots to perform complex tasks that require a nuanced understanding of the tactile environment. In the medical field, multimodal sensors can enhance the capabilities of diagnostic tools and prosthetic devices by providing detailed feedback on touch, pressure, temperature, and even texture. This versatility also opens up possibilities in

consumer electronics, where devices can become more intuitive and responsive to human touch.

2.3.5 Adaptability to Complex Environments

Multimodal tactile sensors excel in adapting to complex and dynamic environments. For example, in the field of soft robotics, where robots interact with unpredictable and variable surroundings, multimodal sensors provide critical data that allows robots to adjust their behavior in real time. This adaptability is crucial for applications like search and rescue operations, where robots must navigate through debris and interact with various materials and surfaces to locate and assist survivors.

2.3.6 Energy Efficiency and Miniaturization

Advances in material science and sensor fabrication techniques have enabled the development of multimodal tactile sensors that are not only highly functional but also energy-efficient and compact. By integrating multiple sensing modalities into a single sensor package, the overall footprint is reduced, and power consumption can be optimized. This is particularly important for wearable devices and portable applications, where size and battery life are critical considerations.

To illustrate the impact of multimodal tactile sensors, several case studies can be considered. In robotics, researchers have developed robotic grippers equipped with multimodal sensors that can delicately handle objects ranging from fragile glassware to complex assemblies. These grippers use combined pressure, temperature, and vibration feedback to adjust their grip dynamically, reducing the risk of damage. In the realm of prosthetics, multimodal tactile sensors have revolutionized the way prosthetic limbs interact with their users. By providing detailed sensory feedback, users can experience a more natural sense of touch, improving their ability to perform daily tasks with greater dexterity and confidence. This advancement has a profound impact on the quality of life for individuals relying on prosthetic devices. Despite the significant advantages, the development of multimodal tactile sensors is not without challenges. Ensuring seamless integration of different sensing modalities while maintaining sensor performance and durability remains a complex task. Additionally, the calibration and interpretation of data from multiple sensors require sophisticated algorithms and processing capabilities.

Looking ahead, ongoing research aims to further miniaturize these sensors, enhance their sensitivity, and develop advanced data fusion techniques to maximize the utility of the multimodal data collected. The integration of artificial intelligence and machine learning with multimodal tactile sensors holds the promise of creating even more intelligent and adaptive systems capable of learning and evolving based on sensory input.

Multimodal tactile sensors represent a significant leap forward in tactile sensing technology. By combining multiple transduction mechanisms, these sensors offer enhanced sensory information, improved accuracy, robustness, versatility, and adaptability. Their impact spans across various fields, from robotics and medicine to consumer electronics, paving the way for more intuitive and responsive systems. As research and development continue to advance, multimodal tactile sensors will undoubtedly play a crucial role in the future of tactile sensing and interaction.

2.4 Characteristics of the proposed Sensor

The sensor proposed in this research work has following attributes:

1. A tactile sensor with a multi transduction mechanism; mimicking human mechanoreception was concepted and fabricated.
2. The capacitive part can respond upto 10N forces in the Normal direction, and up to 1.2N forces in X and Y shear direction.
3. At low frequency forces, the capacitive part retains the same output value and exhibits a linear response while the piezoelectric sensor only fires up at the application or releasing of force.
4. The dynamic force signals up to 60Hz are sensed by the Piezoelectric part, thus giving sensor the capability to respond to higher frequency events happening in surrounding.
5. The sensor design is not only robust but also cost effective and scalable thus making it an ideal fit for integrating with MIRS tools as a low-cost disposable sensor.

2.5 Force requirements for Surgical procedures

As the sensor being proposed in this study is designed with the aim to employ in robotic surgical tools and systems. Therefore, due to variation in different types of surgical procedures the amount of force required for this purpose varies. The detailed force requirements for different surgical procedures and practices are given in Table 2.2.

Table 2.2 Force requirements in different surgical practices [49]

Type of Surgery	**Average Force (N)**	**Maximum Force (N)**
General Surgery	4.67	11.4
Otorhinolaryngology	8.49	15.6
Obstetrics & gynecology	8.69	10.1
Urology	9.79	15.6

Chapter 3: Design, Working Principle and Fabrication of Sensor

This chapter is dedicated to the design, working principle and fabrication of proposed sensor.

3.1 Design of Proposed Sensor

Fig. 1(a) shows the top, bottom, and side views of the capacitive-piezoelectric tactile force sensor. The sensor has been realized as a soft sensing element, sitting on a hard dual sided Printed Circuit Board (PCB) base. Fig. 2 shows the exploded view of the sensor, showing all the respective layers in the sensor. The top layer is a soft dome made from Ecoflex 00-30, which ensures a uniform distribution of the applied force onto the sensor. The second layer is a flexible top circular electrode made of copper sheet. The third layer is a flexible elastomer Ecoflex 00-30 serving as a dielectric medium for capacitor. Beneath the elastomer is a dual layer FR4 PCB, with printed four electrodes on top and a circular electrode on bottom for Piezoelectric attachment. The overall sensing area of the sensor is arranged in a circular geometry with 12mm diameter. Ecoflex laying above the electrodes has 12 mm diameter and 3mm thickness. The position of the capacitive and piezoelectric stack mimics the placement of SA and FA receptors in the human skin.

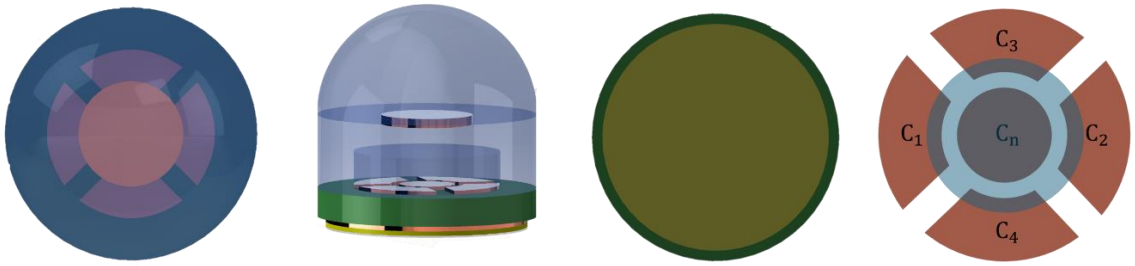

Figure 3.1 (a) top view of the sensor (b) right view of the sensor (c) piezoelectric attached to PCB bottom side (d) top and bottom electrodes symmetry of capacitor.

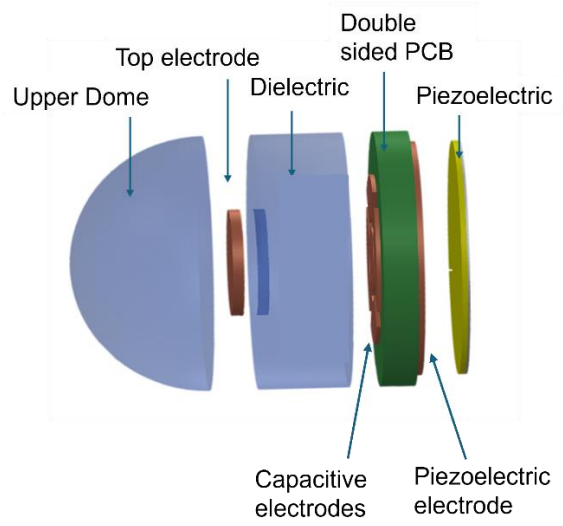

Figure 3.2 Exploded view of the sensor.

3.2 Working Principle of Proposed Sensor

Fig. 3 shows the two-dimensional cross view of the sensor under different loading conditions. Figure 3 (a) shows the sensor profile when no external force is acting, in (b) a normal force is acting on the sensor. Both the capacitive and piezoelectric parts are sensitive to normal loading. Normal force compresses the dielectric and brings the top electrode closer to the bottom electrode and thus an increase in the capacitance, also a normal force acting on the sensor generates the piezo potential. Under the shear loading as shown in the fig. 3(c) only capacitive part responds to the shear loading whereas the top electrode displaces and the overlapping area of the top electrode with the bottom electrode changes, thus contributing to the change in capacitance and eventually helps in force measurement.

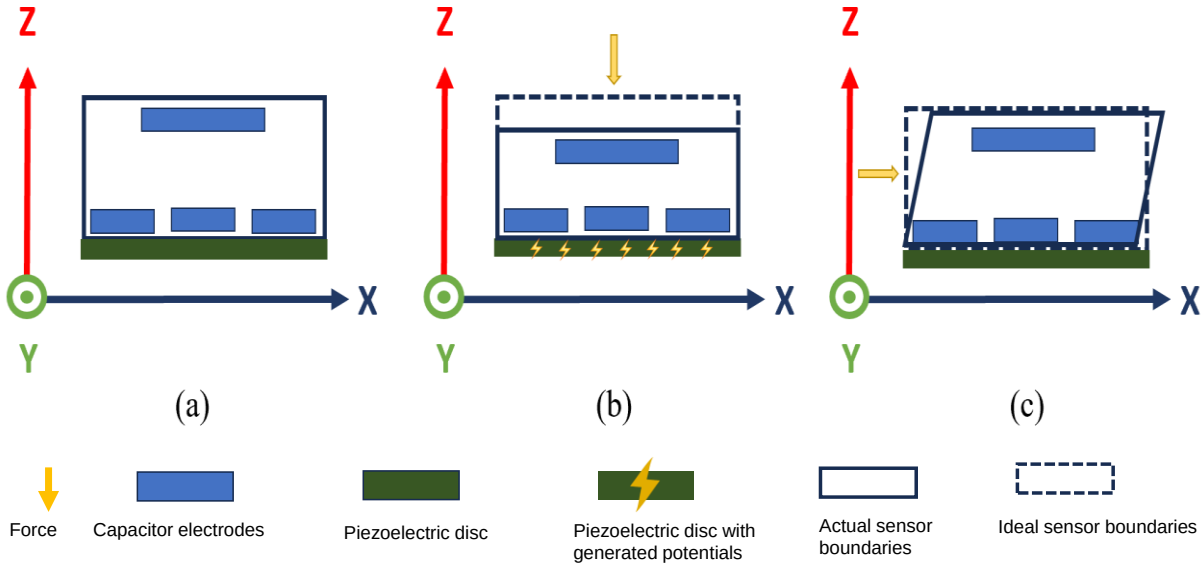

Figure 3.3 Cross section view of the sensor under different loading conditions (a) no loading (b) normal loading (c) shear loading

3.3 Fabrication of Sensor

The whole sensor stack was realized by rapid prototyping fabrication techniques, ensuring that the whole fabrication process could be easily followed sustaining that sensor remains economical too. For the upper dome and the elastomeric dielectric layer Ecoflex 00-30 was procured from SmoothOn Ecoflex 00-30 Inc., Macungie, PA, USA. The elastomer is available in two parts A and B, which need to be mixed in equal ratios 1:1. After taking equal amounts of both parts, the mixture was thoroughly stirred to ensure homogenous mixing. The air molecules which got entrapped in the mixture while mixing was eliminated by degassing the mixture. After this, the mixture was poured into mold for drying and casting. The molds of the requisite dimensions were modelled, and 3D printed with Polylactic Acid (PLA). The copper upper electrode was etched out of a flexible copper sheet. To ensure the proper positioning of the electrode over the bottom electrode, an alignment mark was added onto the drying mold, resulting in an etched-out dielectric having an impression for positioning of the

top electrode. PCB was fabricated on FR4 substrate. The piezoelectric disc was attached onto the PCB electrode via a Silver Conductive Epoxy. The elastomers were glued on to the PCB. Fig. 3.4 shows the actual fabricated sensor.

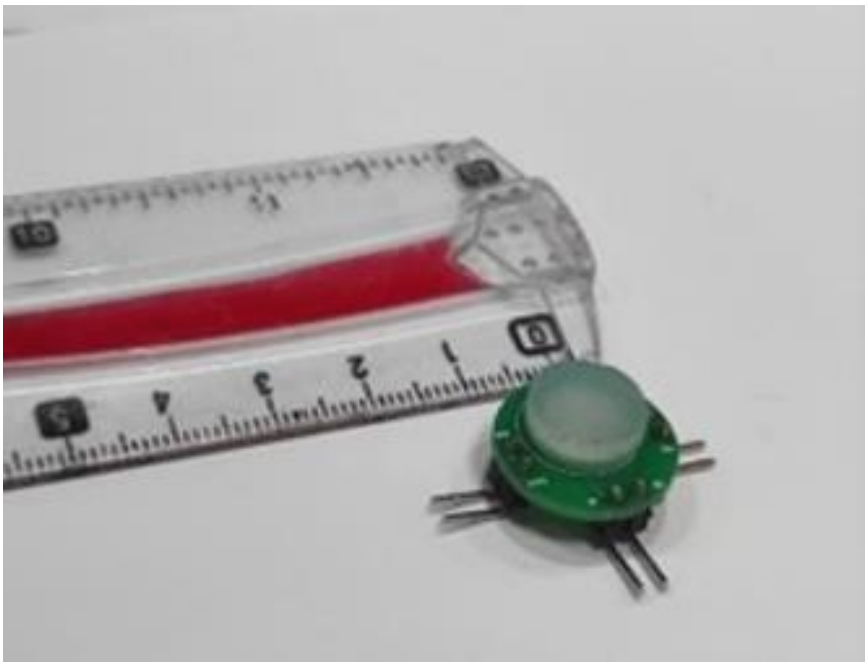

Figure 3.4 Fabricated Sensor

Chapter 4: Mathematical Modelling

As per the discussion of the general working principle of the sensor, the fabricated sensor can detect normal and shear input static with the help of capacitive part and dynamic forces with the help of piezoelectric part. To describe the overall behavior of the sensor a mathematical model has been presented. This section covers the mathematical modelling of piezoelectric and capacitive parts of the sensor:

4.1 Mathematical model of piezoelectric part:

According to the nature of piezoelectric materials, the force applied to the sensor results in a dipole moment within the piezoelectric material due to its non-centrosymmetric property. This results in the generation of the piezo potential. The relationship between the applied force and the charges generated can be derived by using two basic relations:

a) *Piezoelectric constituent equation*

b) *Generalized equation for parallel plate capacitor.*

Starting from the piezoelectric constituent equation, following relationship between the polarization and stress can be derived.

$$\boldsymbol{P = dX} \quad \text{(I)}$$

here, *P* is the *Polarization*, *d* is the *piezoelectric coefficient* dependent on the material and *X* is *stress.*

The second equation that can help is equation for parallel plate capacitor:

$$\boldsymbol{Q = CV} \quad \text{(II)}$$

Here, *Q* is the *charge*, *C* is *Capacitance* and *V* is the generated *Voltage.*

The final equation can be derived by using these two relationships, the polarization can also be defined as the charges produced per unit area.

$$\boldsymbol{P = Q/A} \quad \text{(III)}$$

Where *A* is the *area*. Also, according to the laws of mechanics, Stress can be equated as Force acting upon Area.

$$\boldsymbol{X = F/A} \quad \text{(IV)}$$

Substituting polarization and stress back in the first equation:

$$\boldsymbol{Q = dF} \quad \text{(V)}$$

Since we are using the piezoelectric sensor in the thickness mode, so d will be replaced by the d33 coefficient, so we can write the equation as:

$$\boldsymbol{Q = d_{33}F} \quad \text{(VI)}$$

As in the sensing application the output quantity that is subjected to change and is being read by the DAQ system is the voltage so equating this equation VI with equation II:

$$\boldsymbol{CV = d_{33}F} \quad \text{(VII)}$$

The equation for parallel plate capacitor is:

$$\boldsymbol{C = \frac{\in_0 \in_r A}{d}} \quad \text{(VIII)}$$

Where A is the area and d is the thickness of the piezoelectric sensor, all are known parameters, relative permittivity of air is a known constant $\mathbf{8.85 \times 10{-}12\ Fm{-}1}$. The other constants are already specified in the datasheet of the piezoelectric material.

Equating equations VII and VIII together:

$$\boldsymbol{d_{33}F = \frac{\in_0 \in_r A}{d} \times V} \quad \text{(IX)}$$

Rearranging,

$$\boldsymbol{V = \frac{d_{33}Fd}{\in_0 \in_r A}} \quad \text{(X)}$$

From the above equation following relation between the voltage and the force can be derived:

$$\mathbf{V} \propto \boldsymbol{F} \quad \text{(XI)}$$

So, greater the forces greater will be the generated piezo potentials.

4.2 Mathematical model of the capacitive part:

For deriving the mathematical model of the capacitive part, stating the equation for the capacitance change in the case of the parallel plate capacitive structure.

$$C = \frac{\in_0 \in_r A}{d} \quad \text{(XII)}$$

Where C is the capacitance, $\in_0$ is a constant; relative permittivity of the air, $\in_r$ is the relative permittivity of the dielectric medium. A is the overlap area of the electrodes and d is the distance between the electrodes.

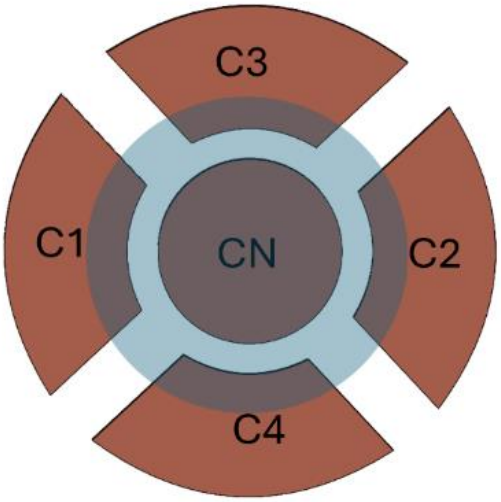

Figure 4.1 Top and bottom electrodes symmetry of capacitor.

The above image shows the symmetry of the electrode's arrangement in the bottom layer. This section covers finding the capacitance change on the application of.

1. Normal force.
2. Shear force.

4.2.1 Capacitance change on the application of Normal Force:

Upon the application of perfect normal force $F = [F_x, F_Y, F_z] = [0,0,F]$ there is no change in the overlap area of the electrodes, so the only parameter contributing to the change of the capacitance is the distance d between the electrodes. The central electrode C_n, is completely shadowed by the top electrode, so the overlap area between the top and C_n electrode does not change even upon the application of shear forces, just giving a way to accurately measure the change in capacitance only due to the change in the distance between the plates, as the area will remain constant, no matter in what direction the force is applied.

Now for solving the change in capacitance for the C_n capacitor, the overlap area is a constant so the change in capacitance reduces to a function of d only.

$$C \propto {}^{1}/_{d} \quad \text{(XIII)}$$

Since the top and bottom electrode both are circles, let the radius of the top electrode R and the radius of the bottom $C_n$electrode plate be r. The overlap area in the case will be πr^2, as the bottom electrode is completely covered by the top electrode.

Thus, the initial capacitance will be:

$$\boldsymbol{C_{n_{initial}}} = \frac{\in_0 \in_{r*} \boldsymbol{\pi r^2}}{\boldsymbol{d_1}} \quad \textbf{(XIV)}$$

Let the initial distance between the plates d_1 equal to the height of electrode. After the application of $F = [F_x, F_Y, F_z] = [0,0,F]$, the distance between the two electrodes will be reduced, let the second distance be d_2, then the capacitance value becomes.

$$\boldsymbol{C_{n_{final}}} = \frac{\in_0 \in_{r*} \boldsymbol{\pi r^2}}{\boldsymbol{d_2}} \quad \textbf{(XV)}$$

Thus, the change in the capacitance can find as:

$$\Delta \boldsymbol{C_n} = \boldsymbol{C_{n_{final}}} - \boldsymbol{C_{n_{initial}}} \quad \text{(XVI)}$$

$$\Delta \boldsymbol{C_n} = \frac{\in_0 \in_{r*} \boldsymbol{\pi r^2}}{\boldsymbol{d_2}} - \frac{\in_0 \in_{r*} \boldsymbol{\pi r^2}}{\boldsymbol{d_1}} = \in_0 \in_{r*} \boldsymbol{\pi r^2} \left(\frac{\mathbf{1}}{\boldsymbol{d_2}} - \frac{\mathbf{1}}{\boldsymbol{d_1}}\right) \quad \text{(XVII)}$$

Likewise for the modelling the change in capacitance for the C_1, C_2, C_3 and C_4 when normal force is acting, we first need to find out the overlapped area for these capacitors.

4.2.2 Overlapping area Calculation for the side capacitors:

According to the symmetry of the capacitor plates, under the no force condition the top electrode just covers a fraction of the area of the bottom electrodes. The shape of the electrodes at the side can be approximated as section of annulus. For one bottom electrode:

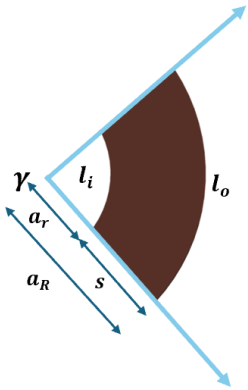

Figure 4.2 Bottom electrode plate approximated as Annulus sector

Where;

γ is the central angle, l_i and l_o are the arc lengths of the respective inner and outer arcs, a_R and a_r are the radius of the inner and outer circles measured from the center, s is the side length of the annulus sector, the following relationship holds:

$$\boldsymbol{s = a_R - a_r} \quad \textbf{(XVIII)}$$

The following equation can be written for the area calculation for the above-mentioned geometry:

$$\boldsymbol{Area = \frac{\gamma}{360} * \pi * (a_R^2 - a_r^2)} \quad \textbf{(XIX)}$$

Now according to the geometry of the sensor, the top plates sit over the bottom plate in a manner that there is a partial overlap of the area between the top electrode and the bottom outer sets of electrodes namely C_1, C_2, C_3 and C_4. Considering the normal state when there is no external force applied,

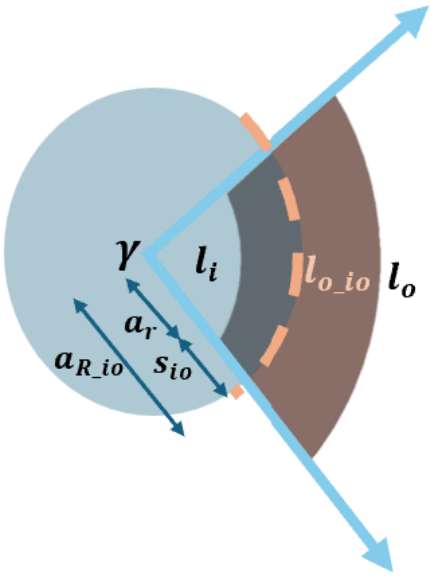

Figure 4.3 Overlapped region of top and bottom side electrode

Here the l_{o_io} is the arc length of the outer arc, laying on the circumference of the overlapped area of the electrode, likewise a_{R_io} and s_{io} are the length of the overlapped region.

so, the above equation can be rewritten as:

$$\boldsymbol{Area = \frac{\gamma}{360} * \pi * (a_{R\_io}^2 - a_r^2)} \quad \textbf{(XX)}$$

Plugging in the calculated area back into the capacitance equation:

$$\boldsymbol{C_i = \frac{\in_0 \in_r * \pi * \gamma * (a_{R\_io}^2 - a_r^2)}{d_1 * 360}} \quad \text{(XXI)}$$

$$i = 1,2,3,4$$

Now on the application of the normal force only the distance d changes so let the new distance b d_2, so the change in capacitance value can be calculated as:

$$\boldsymbol{\Delta C_i = \frac{\in_0 \in_r * \pi * \gamma * (a_{R\_io}^2 - a_r^2)}{360} * (\frac{1}{d_1} - \frac{1}{d_2})} \quad \text{(XXII)}$$

$$i = 1,2,3,4$$

4.2.3 Capacitance change on the application of Shear Force:

Considering the ideal situation with no fabrication errors and the top plate centrally aligned over the bottom plates such that the central electrode is completely shadowed, and the outer boundary electrodes have an equal overlapped area. A shear force in any planar direction $F = [F_x, F_Y, F_z] = [F, 0,0]$ or $F = [F_x, F_Y, F_z] = [0, F, 0]$ changes the overlap area of the outer electrodes in the requisite direction while the central plate remains indifferent to top plate positioning. Let the initial overlapping area as calculated by equation number (XX) be A_1, that is defined by the following equation:

$$\boldsymbol{A_1 = \frac{\gamma}{360} * \pi * (a_{R\_io}^2 - a_r^2)} \quad \text{(XXIII)}$$

Now on the application of the shear force the overlapped area will change from A_1 to A_2. After the application of the force in a requisite direction the top plate will move in the direction of force and thus the overlapped area will change owing to the changes in s_{io} and a_{R_io}. As shown in the above figure on the application of shear force in X direction, the side length of the overlapped annulus segment and the radius of the outer arc of overlapped region will both change by a factor, let the factor be δs and δa_R. So,

$$\boldsymbol{\Delta s = s_{io} + \delta s} \quad \text{(XXIV)}$$

$$\boldsymbol{\Delta a_R = a_{R\_io} + \delta a_R} \quad \text{(XXV)}$$

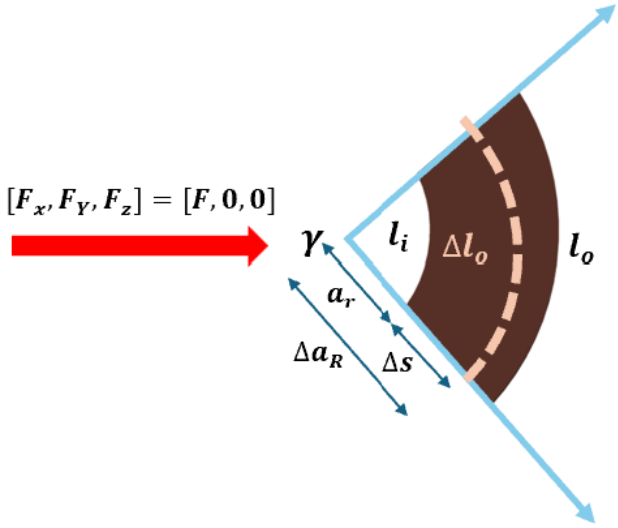

Figure 4.4 Overlapping area changes over shear force application

So, this changes the area to A_2, which becomes:

$$\boldsymbol{A_2 = \frac{\gamma}{360} * \pi * (\Delta a_R^2 - a_r^2)} \quad \text{(XXVI)}$$

Thus, the capacitance will become.

$$\boldsymbol{C_2 = \frac{\in_0 \in_r * \pi * \gamma * (\Delta a_R^2 - a_r^2)}{d * 360}} \quad \text{(XXVII)}$$

As the sensor is symmetric so for the rest of the electrodes in the bottom plate the above equation holds valid.

So;

$$\boldsymbol{C_{2\_i} = \frac{\in_0 \in_r * \pi * \gamma * (\Delta a_R^2 - a_r^2)}{d * 360}} \quad \text{(XXVIII)}$$

$$i = 1,2,3,4$$

For finding the change in the capacitance value due to applied shear force.

$$\boldsymbol{\Delta C = C_2 - C_1} \quad \text{(XXIX)}$$

$$\Delta \boldsymbol{C_i} = \frac{\in_0 \in_r * \boldsymbol{\pi} * \boldsymbol{\gamma}}{\boldsymbol{d} * \boldsymbol{360}} * \left(\left(\Delta \boldsymbol{a_R^2} - \boldsymbol{a_r^2}\right) - \left(\boldsymbol{a_{R_{io}}^2} - \boldsymbol{a_r^2}\right)\right) \quad \text{(XXX)}$$

$$i = 1,2,3,4$$

Solving this.

$$\Delta \boldsymbol{C_i} = \frac{\in_0 \in_r * \boldsymbol{\pi} * \boldsymbol{\gamma}}{\boldsymbol{d} * \boldsymbol{360}} * \left(\boldsymbol{\delta a_R^2} + \boldsymbol{2 a_{R_{io}}} * \boldsymbol{\delta a_R}\right) \quad \text{(XXXI)}$$

$$i = 1,2,3,4$$

According to the geometry upon the application of the force in positive X direction; C_1 decreases and C_2 increases, likewise upon the application of force in the negative Y direction; C_3 decreases and C_4 increases, while C_n remains unchanged.

Chapter 5: FEM Modelling

The Finite Element Method (FEM) is an indispensable computational technique in the realm of engineering, renowned for its versatility and precision in solving complex problems that involve a range of physical phenomena, including structural mechanics, thermodynamics, electromagnetism, and fluid dynamics. In the context of sensor design and analysis, FEM serves as a powerful tool for predicting the behavior of a sensor under various operating conditions. It provides a detailed understanding of how a sensor responds to mechanical, electrical, thermal, and other environmental factors, which is crucial for ensuring the reliability and functionality of the sensor in real-world applications.

FEM allows engineers to create a virtual prototype of the sensor, simulating its performance in a controlled, yet highly realistic environment. This approach offers significant advantages over traditional methods, as it enables the verification of theoretical models before any physical prototypes are constructed. By identifying potential design flaws, optimizing sensor parameters, and exploring the effects of different materials and geometries, FEM helps to reduce development costs and accelerate the design process. Additionally, it provides insights into the sensor's limitations and operational boundaries, ensuring that the final product meets the required performance standards.

In this chapter, we delve into the FEM simulations conducted to validate the mathematical model of a capacitive-piezoelectric tactile force sensor designed for use in minimally invasive robotic surgeries (MIRS). This sensor, which combines capacitive and piezoelectric sensing mechanisms, is intended to measure both static and dynamic forces with high precision. The dual-mode operation of the sensor necessitates a comprehensive analysis of its behavior under different loading scenarios, including normal and shear forces, as well as static and dynamic conditions. The simulations carried out in this study are crucial for evaluating the sensor's ability to accurately measure these forces and for understanding the interplay between its capacitive and piezoelectric components.

The FEM simulations were performed using COMSOL Multiphysics, a sophisticated software platform that integrates multiple physical domains, enabling the simulation of complex systems with interacting phenomena. The simulations aimed to assess several key aspects of the sensor's performance, including the sensitivity and linearity of the capacitive sensing mechanism, the voltage response of the piezoelectric component, and the overall structural integrity of the sensor under applied forces. By replicating the conditions under which the sensor will operate in a surgical environment, the FEM analysis provides a detailed evaluation of the sensor's design, ensuring that it can deliver the required performance with consistency and accuracy.

One of the primary goals of the FEM simulations was to validate the mathematical model that underpins the sensor's design. This model, developed in earlier chapters, provides a theoretical framework for understanding how the sensor's capacitive and piezoelectric elements respond to external forces. However, theoretical models are often based on assumptions and simplifications that may not fully capture the complexities of real-world behavior. FEM simulations, on the other hand, offer a more nuanced and detailed analysis by accounting for factors such as material non-linearities, geometric imperfections, and coupled field interactions. As such, the simulations serve as a critical step in bridging the gap between theory and practice, ensuring that the sensor design is both robust and effective.

Moreover, the FEM simulations provide valuable insights into the sensor's performance across a range of scenarios that may be difficult or impossible to replicate in physical experiments. For example, the simulations allow for the exploration of extreme loading conditions, such as high shear forces or rapid dynamic changes, which could reveal potential vulnerabilities or performance limitations. Additionally, by simulating the sensor's response over a wide range of frequencies, the analysis helps to determine the sensor's bandwidth and its suitability for detecting high-frequency events, such as vibrations or rapid tissue movements during surgery.

5.1 Material Properties

In the Finite Element Method (FEM) simulation of the capacitive-piezoelectric tactile force sensor, the accurate definition of material properties is crucial for obtaining reliable and realistic results. The materials used in the sensor play a significant role in determining its mechanical and electrical behavior, particularly in how it responds to applied forces.

5.1.1 Elastomeric Dielectric Material

The dielectric material forms a critical part of the capacitive sensing mechanism. In this study, a blank elastomeric material was created to serve as the dielectric layer between the electrodes. This material was chosen for its flexibility and high permittivity, which are essential for accurate force measurement in the sensor.

The following material properties were assigned to the elastomeric dielectric:

- **Density**: The density of the elastomer was set to 1070 kg/m³. This value is typical for elastomeric materials, which are often used in flexible electronic applications due to their lightweight and compliant nature. The density influences the overall mass and inertia of the sensor, which are important factors in dynamic simulations.
- **Young's Modulus**: The Young's modulus of the elastomer was defined as 0.1 MPa. This relatively low modulus indicates that the material is highly flexible, allowing it to deform easily under applied forces. The flexibility of the dielectric material is crucial for ensuring that the sensor can detect small changes in pressure and shear forces, as the deformation of the dielectric layer directly affects the capacitance between the electrodes.
- **Relative Permittivity (Dielectric Constant)**: The relative permittivity of the elastomer was set to 2.8. This parameter is critical for the capacitive sensing mechanism, as it determines the material's ability to store electrical energy in the presence of an electric field. A higher permittivity enhances the sensor's sensitivity to changes in force, as it increases the capacitance for a given electrode configuration.
- **Poisson's Ratio**: The Poisson's ratio of the elastomer was set to 0.49. This value, close to the incompressible limit of 0.5, indicates that the material experiences minimal volume change under mechanical deformation. This property is beneficial for maintaining consistent sensor performance, as it ensures that the dielectric layer maintains its thickness and surface area, which are crucial for stable capacitance readings.

The selection of these material properties for the elastomeric dielectric was based on the need for a material that is both mechanically compliant and electrically responsive, enabling the sensor to accurately measure small forces with high sensitivity.

5.1.2 Copper Electrodes

Copper was chosen as the material for the electrodes due to its excellent electrical conductivity and mechanical properties. Copper is widely used in electronic components for its ability to efficiently conduct electricity with minimal resistance, making it an ideal choice for the sensor's electrodes.

The key material properties of copper used in the simulation include:

- **Density**: The density of copper was set to 8960 kg/m³. This high density reflects the substantial mass of copper relative to other materials, which can influence the sensor's overall weight and its dynamic response in the simulation.
- **Young's Modulus**: The Young's modulus of copper was defined as 110 GPa. This high modulus indicates that copper is a stiff material, providing structural integrity to the electrodes while ensuring minimal deformation under applied forces. The rigidity of the electrodes is important for maintaining consistent spacing between the dielectric layers, which directly impacts the sensor's capacitance.
- **Electrical Conductivity**: Copper's electrical conductivity was set to 5.96 × 10^7 S/m. This high conductivity ensures that the electrodes can efficiently transmit electrical signals with minimal energy loss, which is critical for the accurate measurement of capacitance and piezoelectric voltage.

The use of copper for the electrodes ensures that the sensor can operate with high electrical efficiency and mechanical stability, providing reliable performance in both static and dynamic force measurement scenarios.

5.1.3 FR4 Substrate for PCB

The Printed Circuit Board (PCB) on which the sensor is mounted was modeled using FR4, a composite material commonly used in electronic applications. FR4 is a glass-reinforced epoxy laminate that offers excellent mechanical strength, electrical insulation, and thermal stability.

The following properties were assigned to the FR4 material in the simulation:

- **Density**: The density of FR4 was set to 1850 kg/m³. This value reflects the moderate weight of FR4, which provides a stable platform for mounting electronic components while maintaining a manageable overall weight for the sensor assembly.
- **Young's Modulus**: The Young's modulus of FR4 was defined as 22 GPa. This modulus indicates that FR4 is a relatively stiff material, providing the necessary structural support for the PCB and ensuring that the sensor remains mechanically stable during operation.
- **Relative Permittivity**: The relative permittivity of FR4 was set to 4.4. This higher permittivity compared to the elastomeric dielectric helps to insulate the electronic

components mounted on the PCB, preventing electrical interference and ensuring accurate signal transmission.

- **Thermal Conductivity**: Although not a primary focus in this simulation, FR4's thermal conductivity was also considered, as it affects the sensor's performance in environments where temperature fluctuations are a concern. The low thermal conductivity of FR4 ensures that heat generated during operation does not easily spread, helping to maintain the integrity of the sensor's components.

5.2 Boundary conditions

In the Finite Element Method (FEM) simulations of the capacitive-piezoelectric tactile force sensor, the correct application of boundary conditions is essential to accurately model the sensor's behavior under various operational scenarios. Boundary conditions define how the sensor interacts with its surroundings and how external forces and constraints influence its performance.

5.2.1 Fixed Constraints

Fixed constraints are used in FEM simulations to restrict the movement of certain parts of the model, simulating the conditions where the sensor is anchored or attached to other components in a real-world application. In the context of the capacitive-piezoelectric tactile force sensor, fixed constraints were applied to the following areas:

- **Sensor Mounting Base**: The base of the sensor, typically attached to a larger structure or embedded within a robotic tool, was subjected to fixed constraints. This means that the nodes at the base were restricted from translating or rotating in any direction (X, Y, and Z axes). This constraint simulates the realistic scenario where the sensor base is securely mounted, ensuring that any applied forces result in deformation of the sensor components rather than movement of the entire sensor.

5.2.2 Boundary Loads

Boundary loads represent the external forces applied to the sensor during operation. In the FEM simulation, these loads are crucial for evaluating how the sensor responds to various types of mechanical stress, including normal forces (perpendicular to the sensor surface) and shear forces (parallel to the sensor surface). The following boundary loads were applied:

- **Normal Force Load**: A distributed load was applied to the top surface of the elastomeric dielectric material to simulate a normal force. This force was applied uniformly across the surface to mimic the pressure experienced by the sensor when in contact with an object. The magnitude of this load was varied during the simulation to assess the sensor's sensitivity and linearity in response to different levels of applied force.
- **Shear Force Load**: Shear forces were applied to the top surface of the dielectric material in both the X and Y directions. These forces simulate the lateral pressure that the sensor might experience in real-world applications, such as when sliding over a

surface. The application of shear forces is critical for evaluating the sensor's ability to detect and measure shear stress, which is a key requirement for tactile sensors used in robotic surgery.

- **Dynamic Load**: To assess the sensor's performance under dynamic conditions, a time-varying load was applied in the simulation. This load represents rapidly changing forces, such as those encountered during quick movements or vibrations. The dynamic load was applied in both normal and shear directions to fully evaluate the sensor's response across different frequencies.

5.2.3 Electrical Terminals

In addition to mechanical boundary conditions, the FEM simulation also required the definition of electrical boundary conditions to accurately model the capacitive and piezoelectric elements of the sensor. These conditions include the assignment of electrical terminals and ground points, which are essential for simulating the sensor's electrical behavior under applied forces.

- **Capacitive Terminals**: The copper electrodes in the capacitive sensing component were assigned as electrical terminals. These terminals were defined as points where the electric potential is applied or measured. The top electrode, which faces the applied force, was connected to a voltage terminal, while the bottom electrodes, associated with the PCB, were connected to separate terminals corresponding to the X, Y, and normal force measurement channels. The electrical potential difference between these terminals was used to calculate the capacitance change as the dielectric material deforms under applied loads.
- **Piezoelectric Terminals**: The piezoelectric layer was connected to terminals where the generated voltage due to mechanical stress was measured. The FEM simulation included these terminals to capture the piezoelectric effect, where mechanical deformation results in an electrical potential. The voltage generated at these terminals under various loading conditions was analyzed to assess the piezoelectric sensor's response to dynamic forces.
- **Ground Conditions**: Grounding is critical in FEM simulations to establish a reference potential for the electrical analysis. In this simulation, one side of each capacitive and piezoelectric terminal setup was grounded. This means that the electric potential at these points was set to zero, providing a baseline against which the other terminals' potentials could be measured.

5.3 Multiphysics

To simulate the sensor's behavior, two primary modules within COMSOL were employed:

1. **Electromechanics Module**: This module was used to simulate the capacitive sensing mechanism. It allows for the coupling of structural mechanics (deformation of the sensor) with electrostatics (changes in capacitance). The module provided a comprehensive framework for modeling how mechanical forces alter the electric field distribution between the sensor's electrodes.

2. **Piezoelectric Module**: This module was employed to simulate the piezoelectric response of the sensor. It integrates the mechanical strain and the resulting electrical potential generated within the piezoelectric material, capturing the sensor's ability to detect dynamic forces.

5.4 FEM Results

The FEM results from the multiphysics analysis have been discussed in following sections.

5.4.1 Capacitive Normal Results

For the capacitive part when the normal force was applied onto the sensor, capacitance at all the electrodes increased as the displacement of the top electrode plate changed with respect to the bottom plates, as proposed in mathematical model. Figure 5.1 shows the sensor profile and average capacitance change in all electrodes under application of normal force. As suggested in the mathematical model the increase in the force acting in the normal direction brought out an increase the capacitance values for all the capacitors, thus an increasing curve for all the capacitive values was observed. Results in figure 5.1 shows the displacement profile of the sensor under the normal loading condition and the 5.1 (b) is the plot for capacitance change over an applied force range of 10N.

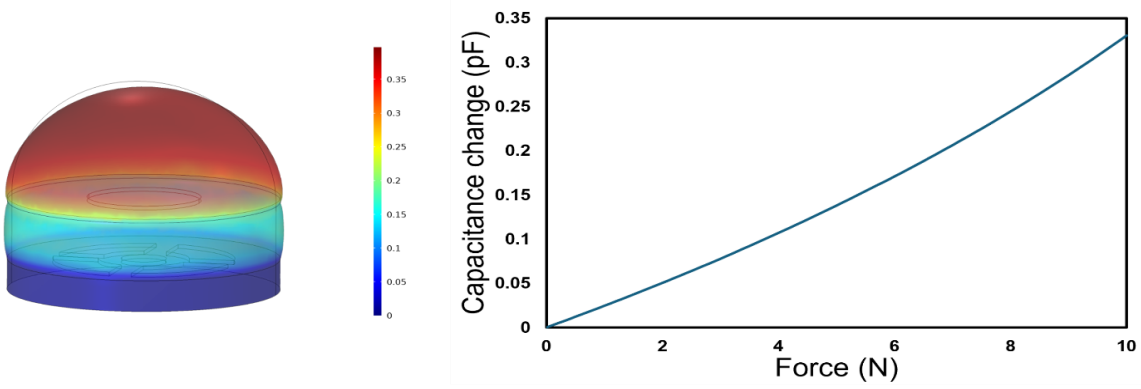

(a) (b)

Figure 5.1 (a) Displacement profile of the sensor under the application of normal force (b) Normalized capacitance change for an applied force in the normal direction.

5.4.2 Capacitive Shear Results

While when the pure shear forces were applied in the +X direction C1 decreased and C2 increased, while the rest of the plates had no change in capacitance value, similarly for the -Y direction force C3 and C4 responded as was suggested by the mathematical model in previous section. Figure 5.2 shows the response of the sensor for a -Y force, normalized capacitance is plotted against Force. Also, according to the design of the sensor the central electrode plate is only sensitive to the normal forces as it is completely overshadowed by the top electrode plate. So the force acting in normal direction deceases the distance between the plates thus contributing to an overall increase in the capacitance value, and when a shear force

is applied the central plate remains unaffected by any changes in the overlap area so the capacitance remains constant and thus the change in capacitance is zero. The lower shear force range is due the physical constraints of the sensor design as further increase in the force values compromises the integrity of sensor.

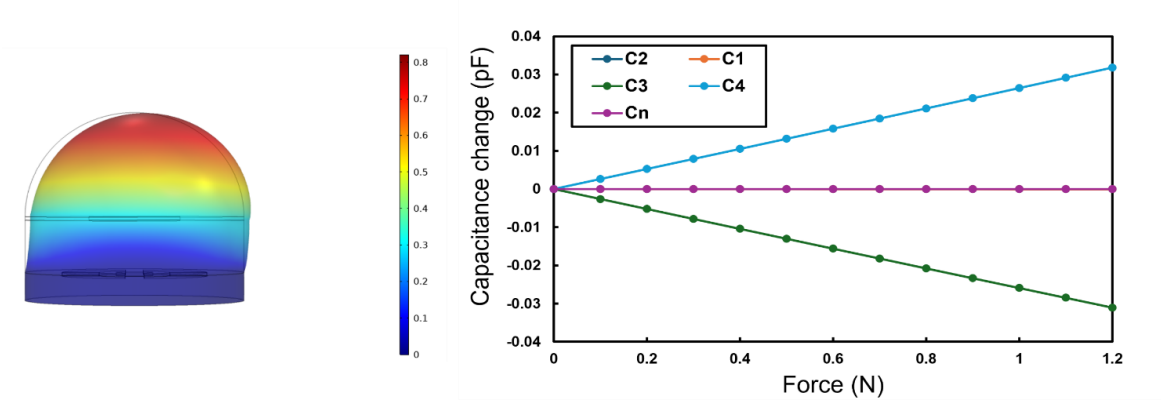

(a) (b)

Figure 5.2 (a) Displacement profile of the sensor under the application of shear force (b) Normalized capacitance change for an applied force in the -y direction.

5.4.3 Piezoelectric

For the Piezoelectric part simulations, the sensor was tested under static and dynamic forces and under low frequency sustained forces. Figure the stress generation and transference to piezoelectric disc under the application of the dynamic forces. As discussed in the boundary conditions the piezoelectric element was simulated as floating potential, to read out the generated potentials in the piezoelectric disc when an external force is applied on it. The particular point of interest was to see that how stresses are being transferred to the piezo element attached to the bottom of the sensor, as the force is applied on the top of the dielectric.

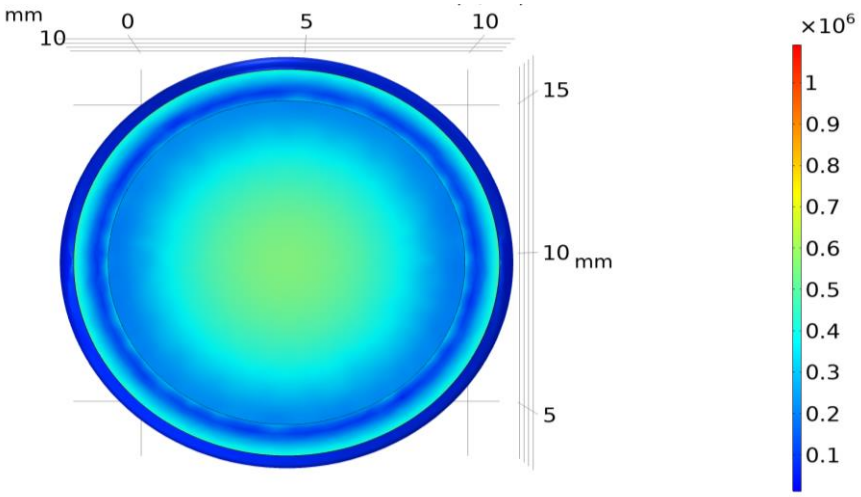

Figure 5.3 Von Misses Stresses generated in the Piezoelectric disc upon force application

The sensor response was evaluated for the piezo potentials on different loading scenario. Theoretically the piezoelectric materials do not respond well to the sustained forces due to the charge equalization over the time, so in order to validate this a step force signal was generated as a piecewise function, for a time range of 0-50s the force remains zero and afterwards it has an amplitude of 1N. The simulated force signal has been shown in figure 5.4.

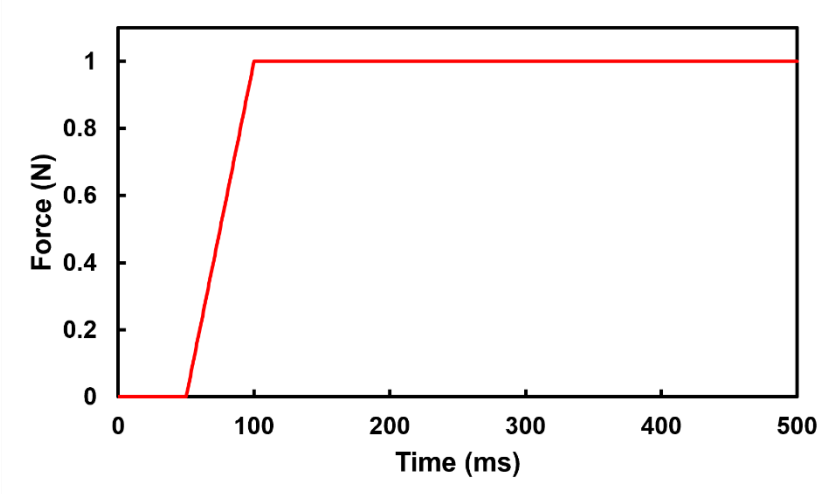

Figure 5.4 Applied piecewise force signal

The sensor's piezoelectric part response validated this concept, the voltage responses generate as long as the force was changing, when the force became constant the generated potentials equalized themselves and the response again became zero thus validating the working principle of sensor.

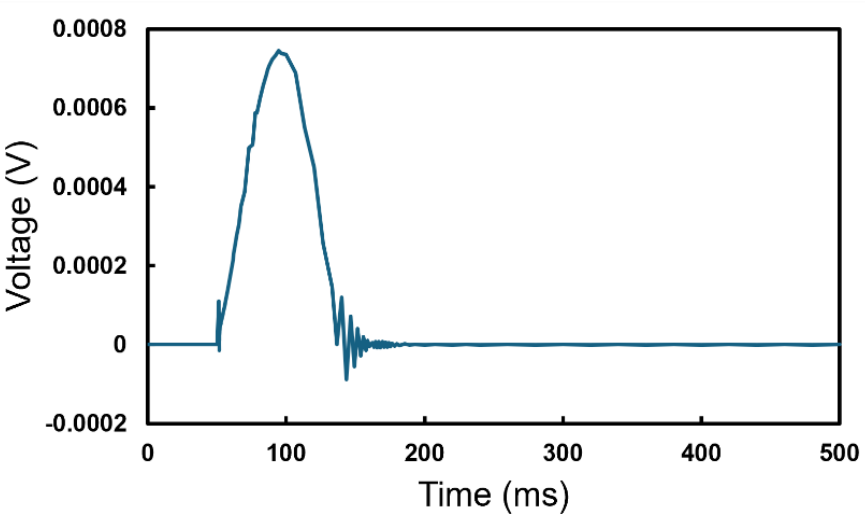

Figure 5.5 Applied piecewise force signal

The FEM simulations conducted in COMSOL Multiphysics were instrumental in validating the mathematical model and ensuring the sensor's design met the required performance criteria. By accurately modeling the sensor's response to various mechanical forces, the simulations confirmed that the sensor could deliver reliable and precise force measurements in both static and dynamic scenarios. These results lay a solid foundation for the physical prototyping and further experimental testing of the sensor.

Chapter 6: Experimental Validation and Results

6.1 Experimental Setup

The static force sensing performance of the sensor was evaluated by applying a force of varying amplitudes using a linear stage motor controlled through a G code. The purpose of using the linear stage motor for the force application was due to its precise control of approximately $1\mu m$ resolution. The force exerted on the sensor was measured using a force gauge that was mounted on the linear stage, the mounting of the force gauge on the linear stage for both the normal and the shear force application has been shown in figure below.

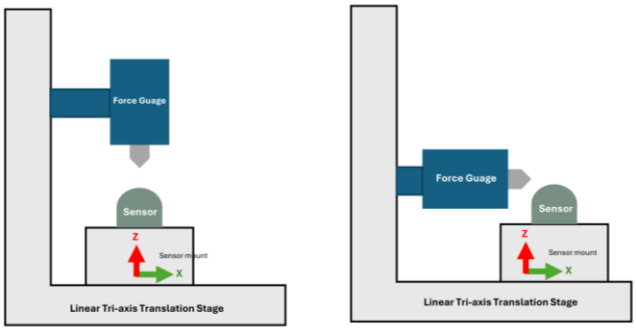

Figure 6.1 Schematics of the experimental setup for static sensor characterization (a) normal force (b) shear force.

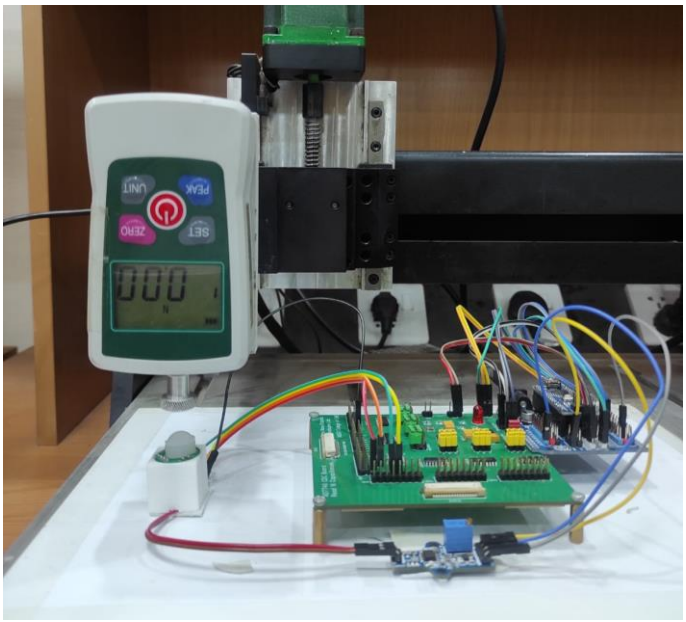

Figure 6.2 Actual experimental Setup for normal force characterization

The dynamic force sensing performance of the sensor was characterized by the Modal Shop Electrodynamic modal shaker TMS2004-E according to the experimental setup as mentioned by Dhaiya et al. [40]. The shaker was capable of applying dynamic forces in the range of 0-11

KHz, it was driven by the GwINSTEK AFG-2012 function generator followed by THE MODAL SHOP SmartAmp power amplifier 2100E21. During the high frequency dynamic forces characterization, the sensor was sandwiched between the shaker and the force gauge. A sensor mount was attached to the shaker and the sensor was attached to it, the force gauge was attached on the same shaker table with a mount, to measure the dynamic forces exerted by the shaker. Figure 5.3 shows schematics of the setup for dynamic forces characterization.

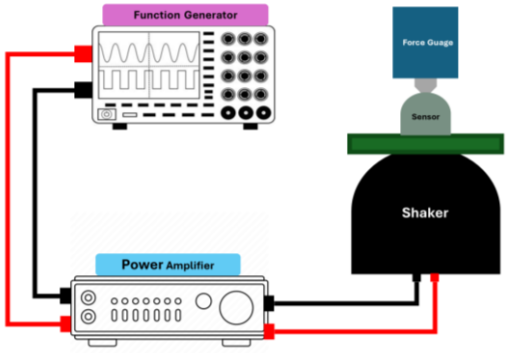

Figure 6.3 Schematics of the experimental setup for dynamic sensor characterization.

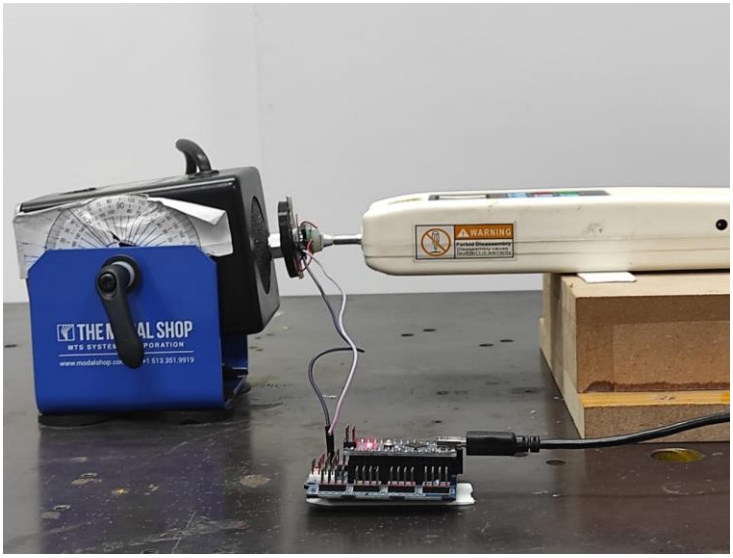

Figure 6.4 Experimental setup for dynamic forces characterization

of the charge amplifier is an analogue signal which is digitized and read with the help of ATmega328P's 10-bit ADC employed by microcontroller MCU (Arduino Nano) at a sampling frequency of ABC. The capacitance change in the capacitors is measured using a 24-bit, 2 channel AD7746 capacitance to digital converter (CDC) having a 4aF resolution. The AD7746 CDC exhibits an accuracy of 4fF. AD7746 ICs were integrated with Arduino Nano Microcontroller. The communication between the MCU and the AD7746 was mediated with the help of Multiplexers.

After digitization by the microcontroller signals from both the sensing elements were sent to a personal computer (PC) via the Universal Asynchronous Receiver/Transmitter (UART) communication, schematics of circuit interface have been shown in figure 10.

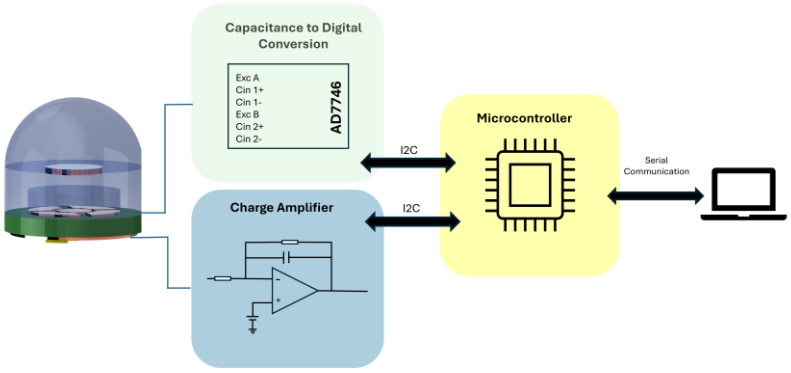

Figure 6.5 Schematics of proposed sensor with the integrated readout strategies.

6.1 Static Loading Characterization:

As explained in the previous section, the piezoelectric part of the sensor exhibits a limitation of charges equalization over the sustained forces. So, in the scenario of static loading, capacitive part of the sensor backs up. For the static force capacitive sensor is sensitive to both the normal and shear forces.

6.1.1 Normal Force Characterization:

Figure below shows the normalized change in capacitance value for the sensor in the normal direction for an input force of 10N. The changes in the capacitance were recorded by AD7746, according to the readout setup mentioned in the previous section. For the further increase in the force value beyond 10N, there was a saturation in the capacitance values as the elastomer could not be compressed beyond that, and the distance between the plates could not be reduced appreciably. The normalized sensitivity of the sensor according to the data plotted is shown in the graph below. The application of the normal force brings about the increase in C_n, C_1, C_2, C_3,and C_4. Thus, the results derived in equation (XXXII) in section 2 are consistent with the results displayed in the above graph. According to the graph, the sensor has a sensitivity of 0.048pF/N in response to the normally directed forces. The sensitivity of the sensor to the normally applied forces is better than the sensitivities 0.0378/N and 0.0192/N reported in [15] and [16].

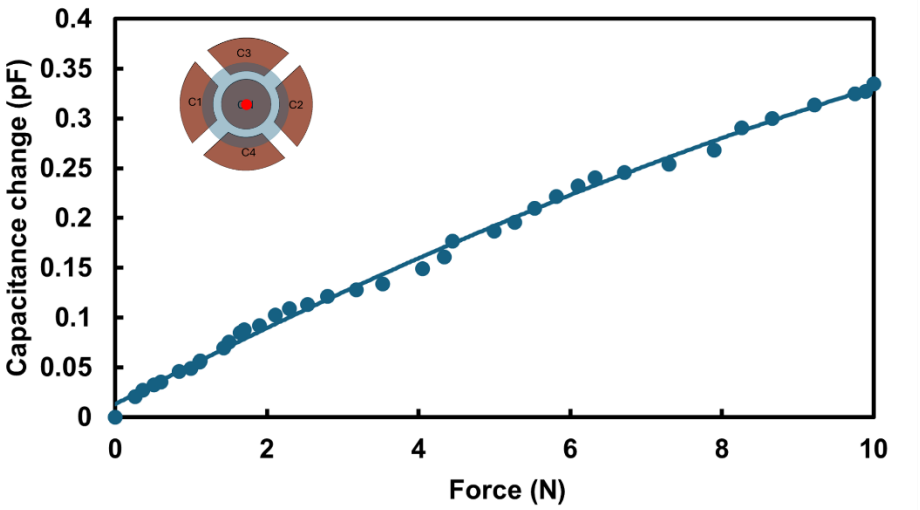

Figure 6.6 Normalized capacitance change for an applied force in the normal direction.

6.1.2 Shear Force Characterization:

For the shear force characterization sensor was mounted onto the linear stage according to the assembly shown in the schematics. As discussed in the mathematical model any planar shear force directed in +X direction will increase the capacitance of C_3 and will decrease the capacitance of C_1. The experimental results are in agreement of the devised model. The sensor exhibits a sensitivity of 0.027pF/N in the X-direction. The sensor is symmetric so the same response can be expected in -X direction. Though ideally there should be no change in C_3, C_4 and C_n, but d errors and errors in the cutting or placement of the upper electrode there is a minute capacitance difference of 0.001pF and 0.003pF respectively, while. $C_n$value remained indifferent to the force applied.

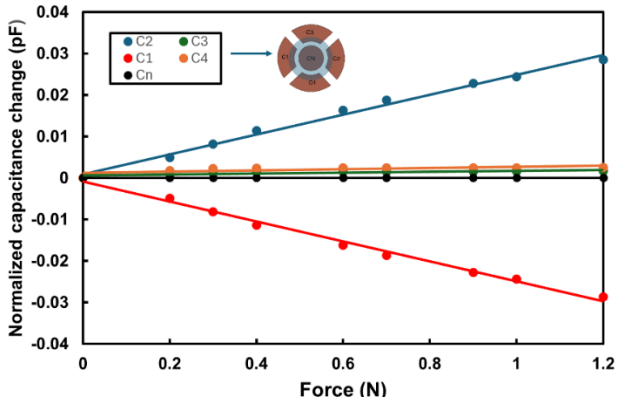

Figure 6.7 Normalized capacitance change over an applied force in the +X shear direction.

Similarly, for a -Y directed force, the response of the sensor has been showed in the figure 8. The C_3 value decreased and C_4value increased consequently, since the pair is acting as a differential pair. Overall the sensor sensitivity obtained from the experimental data for Y direction shear forces is 0.029pF/N. As deduced in the mathematical section that rest of the electrodes $C_1, C_2$and $C_n$should remain neutral to the Y direction shear forces. However, there

were minute changes of 0.00251 and 0.0016 in C_1 and C_2. These little changes can be imparted to the fabrication or alignment errors.

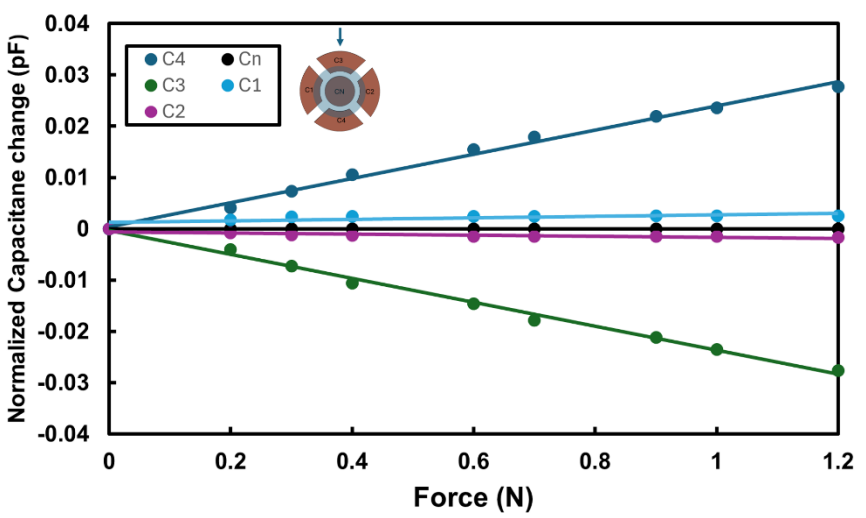

Figure 6.8 Normalized capacitance change over an applied force in the -Y shear direction.

6.2 Low Frequency Loading Characterization:

For quasi-static loading characterization, a custom force square-wave signal was generated having an amplitude of 1N and 1.66Hz frequency was generated as shown in figure 5.9. The force signal was applied through the linearized motor stage and the change in the capacitance and voltages were recorded simultaneously. The capacitive part held the responses effectively over the loading and unloading durations while as expected the piezoelectric sensor responded only over the application and lifting off the force, making it sensitive only to the force changes.

Figure 5.10 the force signal generated and the capacitive and piezoelectric responses acquired by the sensor. The base capacitance values of the capacitor is already very small in the range of pF, also the impedance of the readout circuit for precision reading of the capacitance values, thus the charging and discharging time of these capacitors is around 10 microseconds, and the data is being sampled at 10Hz in the AD7746 evaluation board, so both due to small charging and discharging time of the capacitor and low sampling rate the meticulous details of the charging and discharging of the capacitor are not visible in the graph.

6.3 Dynamic Loading Characterization:

As for the higher frequency dynamic forces the sensor was mounted on the shaker plate as described in the previous section. Sensor was characterized in two fashions:

I. By keeping the force constant and increasing the frequency values
II. By keeping the frequency constant and increasing the force values

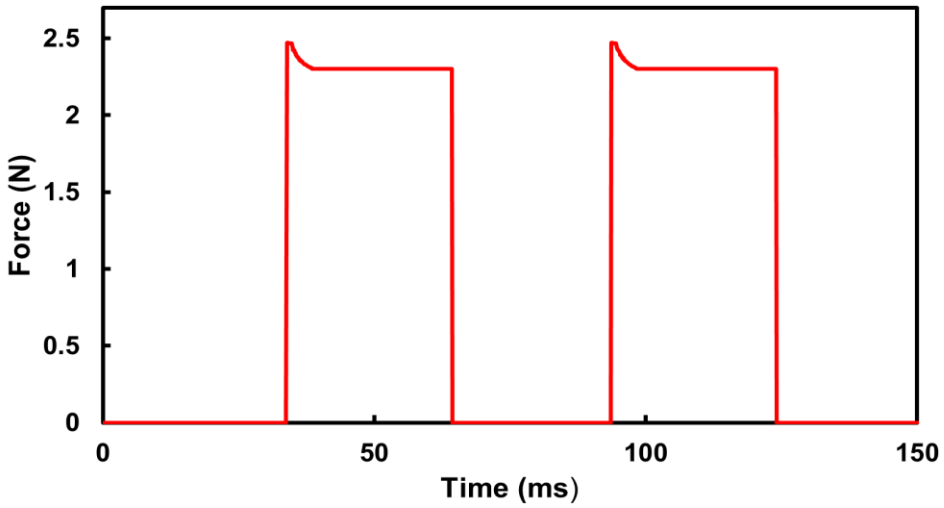

Figure 6.9 Generated force signal of 1.66Hz and 2.5 N

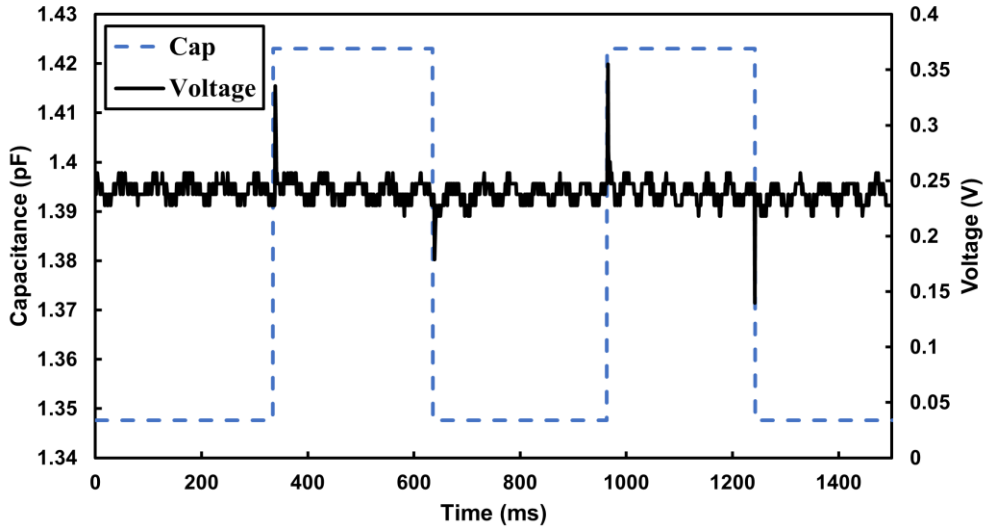

Figure 6.10 Voltage changes for a dynamic force signal of 1.6Hz

In both the scenarios the response of the piezoelectric sensor on the applied dynamic force was evaluated. Figure 6.11 shows the behavior of the piezoelectric sensor to the applied forces at different frequencies, while figure 6.12 shows the behavior of the piezoelectric at a constant 10 Hz frequency and increasing force amplitudes. The experimental data presented in the graph validates the conclusion drawn in the equation (XI). The greater the force magnitude exerted on the sensor the greater peak potential was generated.

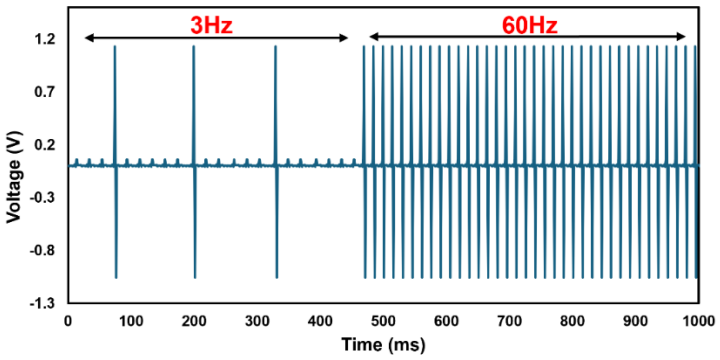

Figure 6.11 Voltage changes for a 4N force captured at different frequencies.

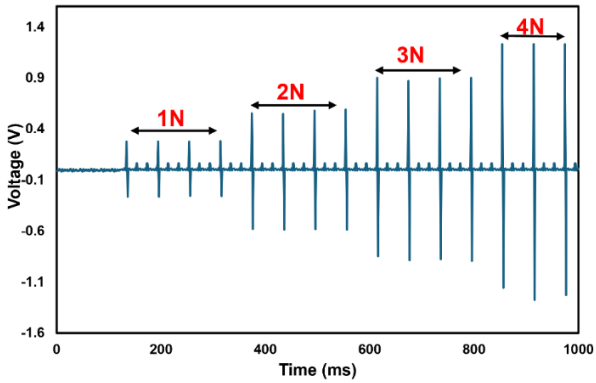

Figure 6.12 Voltage changes for a 10Hz dynamic force signal of varying amplitudes.

Capacitive response was also taken at the application of these high frequency dynamic forces but the change in capacitance was not able to keep up the pace of dynamic signals. As stated earlier the change in the capacitance on normal force is governed by the change in distance $\boldsymbol{d}$ between the top and bottom electrodes, at higher frequencies the compression and relaxation of the dielectric owing to the sensor dimensions could not follow the impact and release of the force, hence rendering no insightful capacitive change at higher frequencies. Thus, making only piezoelectric sensor sensitive to these higher frequency forces.

6.4 Force Estimation based on Experimental data:

Since the sensor is designed to be integrated with MIRS tools, in that realm the sensor will be needed for measuring the forces. So, the output from the capacitive and piezoelectric sensor parts (in the form of the change in capacitance and change in the output voltage) are needed to be converted in forces. For this purpose, the experimental data acquired from the sensor was analyzed in a data analysis software and a linear regression curve was fitted on the data with the maximum R^2 value, ensuring the credibility of the fit. The coefficients of the polynomial equation were obtained. The following relationship of force estimation by the acquired capacitance change in normal direction is given by:

$$\Delta C = 0.0008F^2 + 0.0405F + 1.3039 \qquad \textbf{(XXXIII)}$$

In the shear direction is given by:

$$\Delta C = 0.0071F^2 + 0.038F + 1.2285 \quad \textbf{(XXXIV)}$$

And the force estimation by the piezoelectric sensing part is given by:

$$\Delta V = 0.0092F^2 + 0.2917F + 0.0768 \quad \textbf{(XXXV)}$$

Any of these relationships of force with the capacitance and the voltage can be employed in the feedback controller of the sensor to output the force measured by the sensor. As this mathematical model also tells that if a certain force $\boldsymbol{F}$ is exerted from the outside environment on to the sensor than what will be the respective changes in capacitance and voltages $\boldsymbol{\Delta C}$ and $\boldsymbol{\Delta V}$ from capacitive and piezoelectric part.

To measure the credibility of the forces estimated by the mathematical model the value of the force estimated by the model is plotted alongside the actual force that was exerted on the sensor. The actual forces exerted on the sensor were recorded from the force gauge. The following graphs show the graphs of actual applied and estimated forces from the sensor, from capacitive normal, shear and piezoelectric part. Figure 18 (a) shows the normal force estimation from the change in capacitance having an error of 4.6%, and (b) shows the shear force estimation having an error of 2.5%. Figure 19 shows the force estimation from the change in the voltage by the piezoelectric part has an error of 2.07%. These error values show a close correspondence between the applied and the estimated forces, thus manifesting the accuracy of the force estimation by the model.

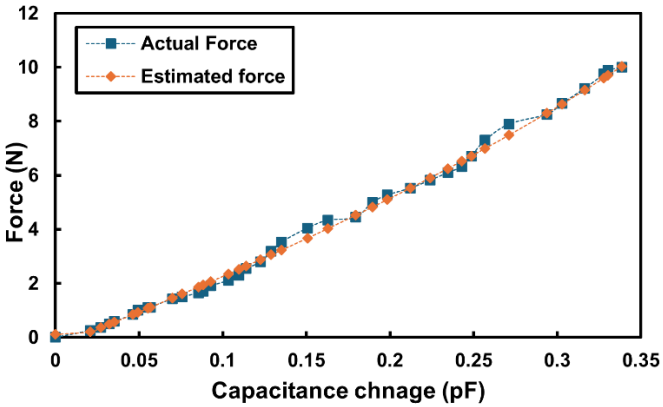

Figure 6.13 Comparison of the applied force and estimated force by the measured capacitance changes for normal force.

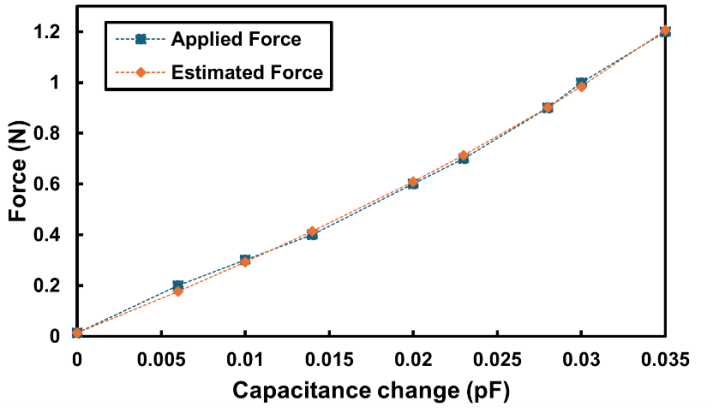

Figure 6.14 Comparison of the applied force and estimated force by the measured capacitance changes for shear force.

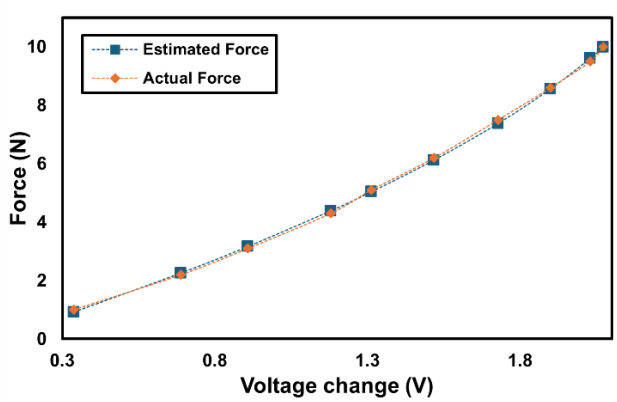

Figure 6.15 Comparison of the applied force and estimated force by the measured voltage changes.

6.5 Repeatability Analysis:

In applications like MIRS, along with accuracy one of the crucial parameters for the sensor's credibility is the repeatability of the sensor. To ensure that the sensor outputs remain consistent over repeated loading conditions and time, four different responses from the sensor were taken under the normal loading conditions at different times over the span of two days. Figure 6.16 shows the repeatability error computed from the capacitive part over the span of four trials is 3.5%.

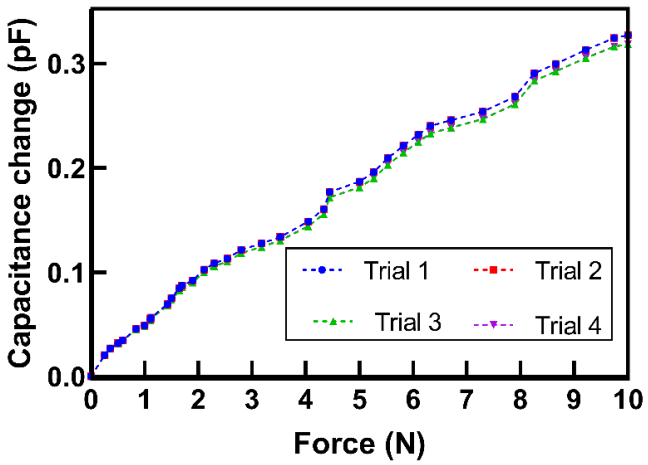

Figure 6.16 Capacitive response of the sensor over four loading trials.

6.6 Validation and Error Mitigation Through Multiple Sensor Fabrication

To mitigate any biases or errors in the sensor results caused by the sensor fabrication, two sensor samples were made identically following the procedures mentioned in the fabrication process section. The two samples were characterized under the normal loading conditions and the capacitance and voltage values were recorded against impact forces. Figure 6.17 shows the variation in the output voltage under impact forces and Figure 6.18 shows the variation in the capacitance values under the normal loading condition.

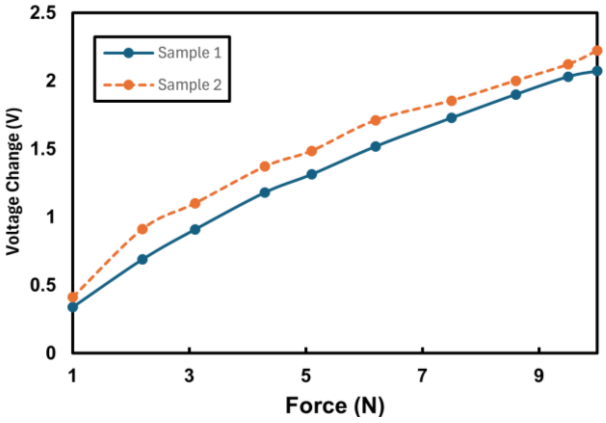

Figure 6.17 The voltage response acquired by two different fabricated sensors.

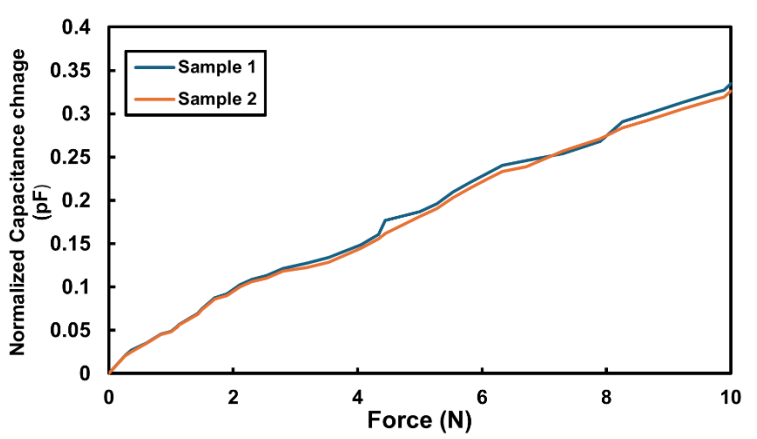

Figure 6.18 Capacitive response acquired by two different fabricated sensors

The above graphs manifest an error of 1.85% in capacitive part and 5.3% in the piezoelectric part negligible to account the errors caused by fabrication of sensor.

6.7 Summary of Performance Characteristics

Upon summarizing the results and performance characteristics of the fabricated sensor, the research can be summarized as follows:

- A tactile sensor with a **multi transduction mechanism** mimicking human mechanoreception was concepted and fabricated.
- The capacitive part can respond to **10N forces** in the **Normal direction**, and up to **1.2N forces** in **X and Y shear direction.**
- At low frequency **quasi-static forces**, the **capacitive part retains the same output value** and exhibits a linear response while the **piezoelectric sensor only fires up at the application or releasing of force.**
- The **dynamic force signals up to 60Hz** are sensed by the Piezoelectric part, thus giving sensor the capability to respond to higher frequency events happening in surrounding.
- The sensor design is not only robust but also **cost effective** and **scalable** thus making it an ideal fit for integrating with MIRS tools as a **low-cost disposable sensor**.

Chapter 7: Sensor Application in Texture Discrimination

7.1 Texture Discrimination in Tactile Sensing:

Texture discrimination refers to the ability to distinguish between different surface qualities, such as roughness, smoothness, and pattern. In the context of tactile sensing, it involves the use of sensors that can mimic the human sense of touch to identify and differentiate between various textures. Tactile sensors, often incorporating technologies such as piezoelectric materials, capacitive sensing, and resistive sensing, are designed to capture detailed information about surface interactions. The concept of tactile sensing has evolved significantly over the past few decades. Initially, research focused on simple pressure sensors that could detect the presence or absence of contact. However, advancements in materials science and sensor technology have enabled the development of more sophisticated tactile sensors capable of capturing nuanced details about texture. Early applications were primarily in robotic manipulation, where the goal was to enable robots to grasp and manipulate objects with human-like dexterity. Various techniques have been developed for texture discrimination, including traditional methods such as optical and acoustic sensing, and more modern approaches leveraging machine learning and advanced signal processing. Optical methods, while effective in some scenarios, are often limited by lighting conditions and surface reflectivity. Acoustic sensing, on the other hand, can be influenced by ambient noise. Tactile sensing, by directly interacting with surfaces, provides a robust and reliable means of texture discrimination, particularly in environments where visual or auditory cues are insufficient.

7.1.1 Importance of Texture Discrimination:

- **Industrial and Robotic Applications**: In industrial automation, texture discrimination is crucial for quality control, enabling machines to detect defects or irregularities in manufactured products. In robotics, texture discrimination enhances the ability of robots to interact with their environment in a more sophisticated manner. For instance, a robot equipped with tactile sensing can adjust its grip on an object based on the detected texture, preventing slippage or damage.
- **Healthcare and Assistive Technologies**: Tactile sensing is also vital in healthcare applications, such as in the development of prosthetics. Prosthetic limbs with integrated tactile sensors can provide users with a sense of touch, improving their ability to perform daily tasks and enhancing their overall quality of life. Additionally, tactile sensing is used in assistive devices for visually impaired individuals, helping them to navigate their surroundings more effectively.
- **Texture Discrimination in Minimally Invasive Robotic Surgeries.** Minimally invasive surgery (MIS) involves performing surgical procedures through small incisions, using specialized instruments and techniques. While MIS offers numerous benefits, including reduced pain, shorter recovery times, and lower risk of infection, it also presents significant challenges for surgeons. The limited visual and tactile feedback in MIS makes it difficult for surgeons to assess tissue properties and navigate the surgical environment effectively. Integrating tactile sensing into robotic surgical

systems can address some of these challenges. Tactile sensors can provide real-time feedback on tissue texture and stiffness, helping surgeons to distinguish between different types of tissues and identify abnormalities. This capability is particularly important in procedures where precise manipulation of delicate tissues is required, such as in neurosurgery or cardiac surgery. For surgeons, enhanced tactile feedback can improve the accuracy and safety of MIS procedures, reducing the likelihood of inadvertent tissue damage. For patients, this translates into better surgical outcomes and faster recovery times. Additionally, the ability to accurately discriminate between tissues can facilitate more effective tumor resections and other complex surgical tasks. The integration of advanced tactile sensing technologies into robotic surgical systems is an area of active research. Future developments may include the use of high-resolution tactile sensors, combined with machine learning algorithms, to provide even more detailed and intuitive feedback to surgeons. These advancements have the potential to revolutionize the field of MIS, making it safer and more effective for a wider range of procedures.

7.2 Experimental Setup

The piezoelectric component was used to analyze and discriminate between different textures using vibrotactile data. The first texture features ridges, while the second is smooth and flat. These textures are affixed to a Linear Tri-axis stage, which systematically displaces linearly over the sensor surface. During this controlled movement, voltage values from the piezoelectric sensor are recorded over a duration of 3 seconds, with 100 data samples collected for each texture sample.

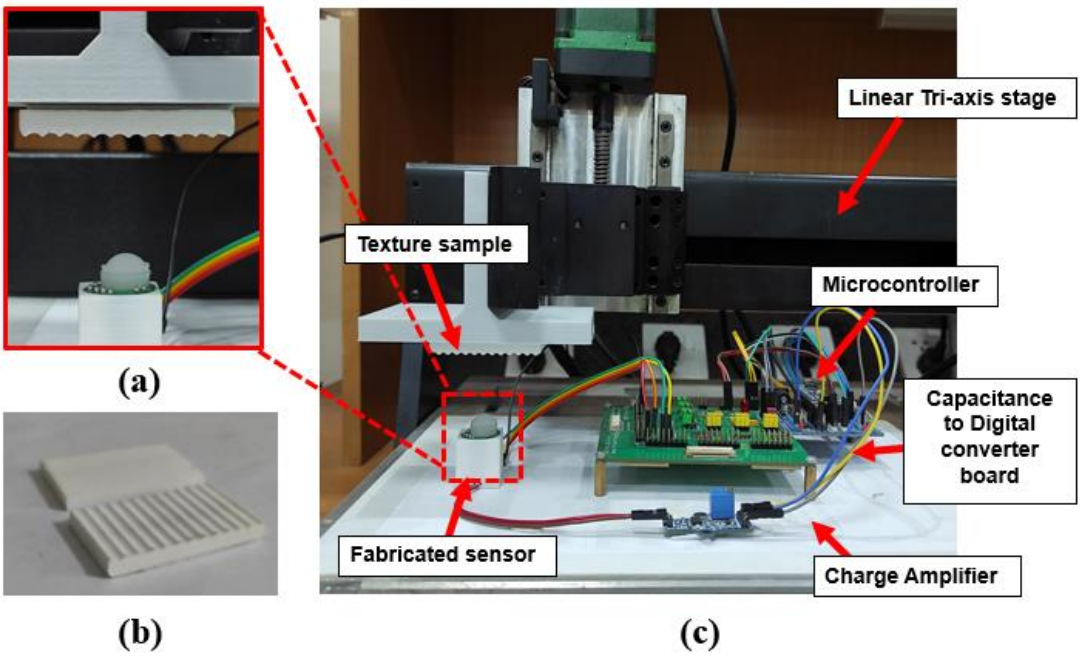

Figure 7.1 (a) Sensor and texture arrangement (b) 3D printed texture samples (c) experimental setup for texture discrimination

7.3 Data Preprocessing

Following the 3-second data collection process involving 100 samples per texture, the recorded voltage signals underwent preprocessing steps to enhance signal quality. Specifically, a bandpass filter was applied to the voltage data to effectively filter out unwanted noise and extraneous frequencies. This filtering step is crucial in refining the captured signals, ensuring that only relevant frequency components associated with tactile information and texture characteristics are retained for subsequent analysis and feature extraction. The filtered data coming from the microcontroller was zero-padded to standardize the length of the time series data to 3000 milliseconds (ms). This uniformity in data length facilitates consistent analysis across different texture samples. Subsequently, the processed data underwent wavelet spectral analysis using a discrete wavelet transform (DWT) with a decomposition level of 1 and employing the Daubechies 4 (db4) wavelet. This spectral analysis technique allows for the extraction of valuable frequency-domain features from the time series data. After wavelet decomposition, a comprehensive set of features was generated to characterize each texture sample. These features included statistical measures such as kurtosis, skewness, zero-crossing rate (zcross), mean, median, root mean square (rms), entropy, variance, and standard deviation (std). These features encapsulate essential characteristics of the vibration signals associated with different textures.

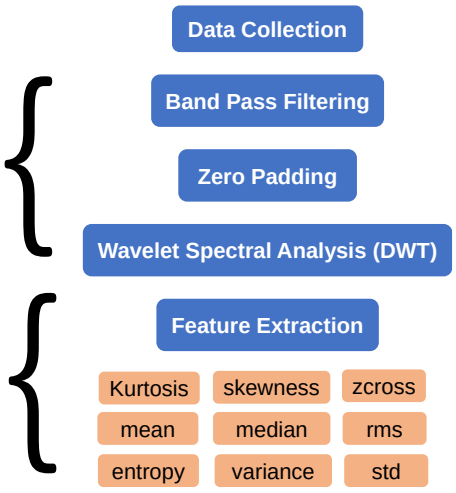

Figure 7.2 Data Processing Architecture

Following feature extraction, a neural network (NN) was employed as the classifier to discriminate between the textured samples based on the extracted features. The NN architecture consisted of an input layer capable of handling 332 features derived from the wavelet analysis. This input layer was followed by three pairs of dense layers, each containing 256 neurons, and dropout layers with a dropout rate of 0.2. The use of dropout layers helps prevent overfitting by randomly deactivating a proportion of neurons during training. The NN classifier was trained using a learning rate of 0.005 and implemented with an 80-20 train-test split. Additionally, a validation set comprising 20% of the training data was used to monitor model performance and prevent overfitting during training. The experimental results of this study demonstrate a high level of accuracy in texture discrimination using the proposed methodology.

During the training phase, the neural network (NN) model achieved a remarkable accuracy rate of 100%, indicating that the model successfully learned the patterns and features associated with the training data. This high training accuracy suggests that the NN effectively captured the underlying relationships between the extracted features and the corresponding texture types within the training dataset. Following the training phase, the model's performance was evaluated using a separate testing dataset and real-time testing was also performed. The testing accuracy of the NN classifier reached an impressive rate of 97.37%. This high testing accuracy indicates the robustness and generalization ability of the trained model in accurately classifying unseen texture samples. The slightly lower testing accuracy compared to the training accuracy suggests that the model effectively learned the underlying patterns from the training data without overfitting, as evidenced by its strong performance on new, unseen data. The observed performance metrics highlight the efficacy of the proposed methodology in utilizing vibrotactile data for texture discrimination. The high accuracy rates achieved through the sensor and the size compliance of the sensor with MIRS tools demonstrate the potential of this methodology for practical applications in palpation and tissue maneuvering during Minimally Invasive Robotic Surgeries.

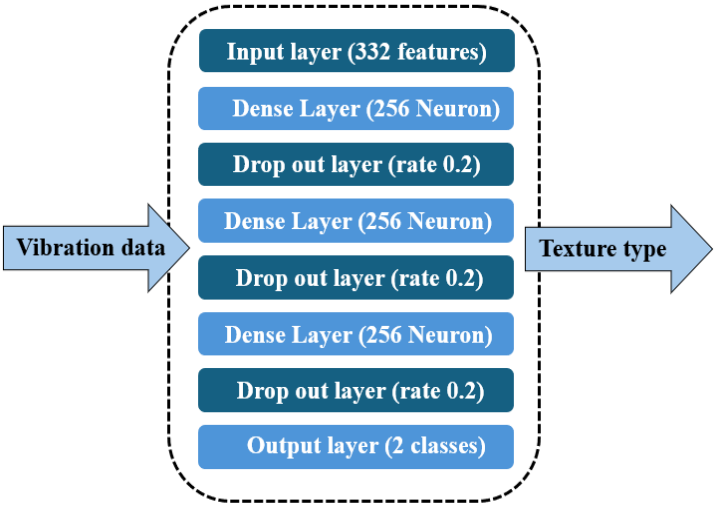

Figure 7.3 Neural Network architecture used for texture classification

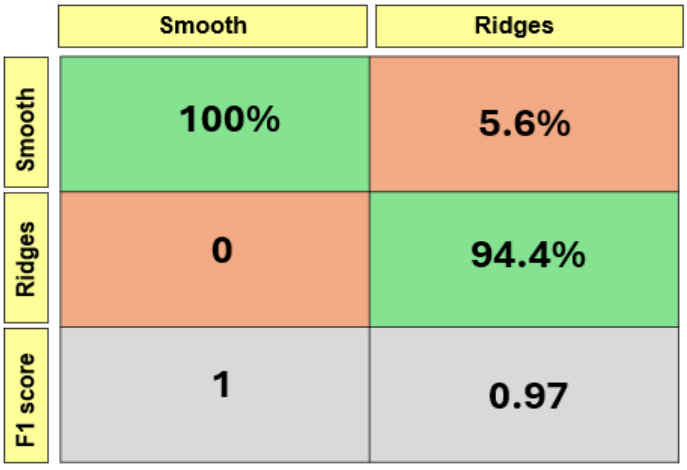

Figure 7.4 Confusion matrix for test data set

Chapter 8: Conclusion

In this study, a tactile sensor with a multi-transduction mechanism—incorporating both piezoelectric and capacitive elements to mimic human mechanoreception—was conceptualized and fabricated. The capacitive component of the sensor can respond to forces up to 10N in the normal direction and up to 1.2N in the X and Y shear directions. At low-frequency quasi-static forces, the capacitive part maintains consistent output values and demonstrates a linear response. In contrast, the piezoelectric sensor activates only upon the application or release of force. This dual-sensor configuration enables the device to detect dynamic force signals up to 60Hz, thereby allowing the sensor to respond to higher frequency events in its environment.

The proposed sensor design, along with the corresponding mathematical model developed, enhances the accuracy and efficiency of force estimation. The robustness, cost-effectiveness, and scalability of the sensor design make it particularly suitable for integration with minimally invasive robotic surgery (MIRS) tools as a low-cost disposable sensor. The sensor's performance metrics, including its repeatability error and the accuracy of force estimation, were thoroughly evaluated to ensure compliance with the stringent requirements of MIRS procedures.

Moreover, the integration of both piezoelectric and capacitive sensing mechanisms provides a comprehensive solution for a wide range of tactile sensing applications. The capacitive sensor's ability to provide steady-state force measurements complements the piezoelectric sensor's responsiveness to dynamic changes, creating a versatile and reliable tactile sensor. This combination is particularly beneficial in surgical environments where both steady and dynamic force feedback are critical for precise manipulation and control.

In summary, the development of this tactile sensor marks a significant advancement in the field of mechanoreception-mimicking devices. Its dual-sensing capability, along with its high accuracy, reliability, and cost-effectiveness, positions it as a valuable component for modern surgical tools and potentially other applications requiring sensitive and precise force measurements. Future work could focus on further miniaturization, enhancing the sensitivity, and exploring additional applications beyond the medical field, such as robotics, prosthetics, and touch-based human-computer interfaces.

References

[1] R. S. Dahiya, G. Metta, M. Valle, and G. Sandini, "Tactile sensing-from humans to humanoids," *IEEE Transactions on Robotics*, vol. 26, no. 1, pp. 1–20, Feb. 2010, doi: 10.1109/TRO.2009.2033627.

[2] B. J. Nelson, I. K. Kaliakatsos, and J. J. Abbott, "Microrobots for minimally invasive medicine," *Annual Review of Biomedical Engineering*, vol. 12, pp. 55–85, Aug. 2010, doi: 10.1146/ANNUREV-BIOENG-010510-103409.

[3] S. Uranüs *et al.*, "Early Experience with Telemanipulative Abdominal and Cardiac Surgery with the Zeus^{TM} Robotic System," *European Surgery*, vol. 34, no. 3, pp. 190–193, Jun. 2002, doi: 10.1046/J.1563-2563.2002.T01-1-02049.X.

[4] G. S. Guthart and J. K. Salisbury, "The Intuitive/sup TM/ telesurgery system: overview and application," *Proceedings 2000 ICRA. Millennium Conference. IEEE International Conference on Robotics and Automation. Symposia Proceedings (Cat. No.00CH37065)*, vol. 1, pp. 618–621, doi: 10.1109/ROBOT.2000.844121.

[5] P. Puangmali, K. Althoefer, L. D. Seneviratne, D. Murphy, and P. Dasgupta, "State-of-the-art in force and tactile sensing for minimally invasive surgery," *IEEE Sensors Journal*, vol. 8, no. 4, pp. 371–380, Apr. 2008, doi: 10.1109/JSEN.2008.917481.

[6] R. Ahmadi, M. Packirisamy, J. Dargahi, and R. Cecere, "Discretely loaded beam-type optical fiber tactile sensor for tissue manipulation and palpation in minimally invasive robotic surgery," *IEEE Sensors Journal*, vol. 12, no. 1, pp. 22–32, 2012, doi: 10.1109/JSEN.2011.2113394.

[7] A. M. Okamura, "Haptic Feedback in Robot-Assisted Minimally Invasive Surgery," *Curr Opin Urol*, vol. 19, no. 1, p. 102, Jan. 2009, doi: 10.1097/MOU.0B013E32831A478C.

[8] T. Zhang, H. Liu, L. Jiang, S. Fan, J. Y.-I. sensors Journal, and undefined 2012, "Development of a flexible 3-D tactile sensor system for anthropomorphic artificial hand," *ieeexplore.ieee.org*, Accessed: Feb. 21, 2022. [Online]. Available: https://ieeexplore.ieee.org/abstract/document/6310004/

[9] V. Maheshwari and R. Saraf, "Tactile Devices To Sense Touch on a Par with a Human Finger," *Angewandte Chemie International Edition*, vol. 47, no. 41, pp. 7808–7826, Sep. 2008, doi: 10.1002/ANIE.200703693.

[10] K. Takei *et al.*, "Nanowire active-matrix circuitry for low-voltage macroscale artificial skin," *Nature Materials 2010 9:10*, vol. 9, no. 10, pp. 821–826, Sep. 2010, doi: 10.1038/nmat2835.

[11] H. Yousef, M. Boukallel, and K. Althoefer, "Tactile sensing for dexterous in-hand manipulation in robotics—A review," *Sensors and Actuators A: Physical*, vol. 167, no. 2, pp. 171–187, Jun. 2011, doi: 10.1016/J.SNA.2011.02.038.

[12] M. I. Tiwana, S. J. Redmond, and N. H. Lovell, "A review of tactile sensing technologies with applications in biomedical engineering," *Sensors and Actuators A: Physical*, vol. 179, pp. 17–31, Jun. 2012, doi: 10.1016/J.SNA.2012.02.051.

[13] S. Najarian, J. Dargahi, and A. Mehrizi, *Artificial tactile sensing in biomedical engineering*. 2009. Accessed: May 08, 2022. [Online]. Available: https://www.accessengineeringlibrary.com/binary/mheaeworks/14b6cc76c087f1ff/80c6d8ec3990c874c07140f32c07c77b57a546e1b236b99b298af07677a257ed/book-summary.pdf

[14] "Robot assisted surgery.jpg - Wikimedia Commons." https://commons.wikimedia.org/wiki/File:Robot_assisted_surgery.jpg#/media/File:Robot_assisted_surgery.jpg (accessed May 08, 2022).

[15] M. H. Lee and H. R. Nicholls, "Review Article Tactile sensing for mechatronics—a state of the art survey," *Mechatronics*, vol. 9, no. 1, pp. 1–31, 1999.

[16] "World Tactile Sensor Market Report 2025 — Teletype." https://teletype.in/@swara/t5X0DvUgR (accessed May 08, 2022).

[17] "Remote Palpation Instrument." http://www.biorobotics.harvard.edu/research/bill.html (accessed May 08, 2022).

[18] S. Khan, S. Tinku, L. Lorenzelli, and R. S. Dahiya, "Flexible tactile sensors using screen-printed P(VDF-TrFE) and MWCNT/PDMS composites," *IEEE Sensors Journal*, vol. 15, no. 6, pp. 3146–3155, Jun. 2015, doi: 10.1109/JSEN.2014.2368989.

[19] D. Kondo, S. Okada, T. Araki, … E. F.-2011 I., and undefined 2011, "Development of a low-profile sensor using electro-conductive yarns in recognition of slippage," *ieeexplore.ieee.org*, Accessed: Feb. 21, 2022. [Online]. Available: https://ieeexplore.ieee.org/abstract/document/6094497/

[20] D. Chathuranga, S. H.-2013 I. International, and undefined 2013, "Investigation of a biomimetic fingertip's ability to discriminate fabrics based on surface textures," *ieeexplore.ieee.org*, Accessed: Feb. 21, 2022. [Online]. Available: https://ieeexplore.ieee.org/abstract/document/6584336/

[21] Y. Zhang, Y. Jen, C. Mo, … Y. C.-I. S., and undefined 2020, "Realization of multistage detection sensitivity and dynamic range in capacitive tactile sensors," *ieeexplore.ieee.org*, Accessed: Feb. 21, 2022. [Online]. Available: https://ieeexplore.ieee.org/abstract/document/9088952/

[22] Y. Liu *et al.*, "A flexible capacitive 3D tactile sensor with cross-shaped capacitor plate pair and composite structure dielectric," *ieeexplore.ieee.org*, Accessed: Feb. 21, 2022. [Online]. Available: https://ieeexplore.ieee.org/abstract/document/9184095/

[23] S. Sokhanvar, M. P.-I. S. Journal, and undefined 2009, "MEMS Endoscopic Tactile Sensor: Toward In-Situ and In-Vivo Tissue Softness Characterization," *ieeexplore.ieee.org*, Accessed: Feb. 21, 2022. [Online]. Available: https://ieeexplore.ieee.org/abstract/document/5290396/

[24] C. Chuang, T. Li, I. Chou, Y. T.-S. and A. A. Physical, and undefined 2016, "Piezoelectric tactile sensor for submucosal tumor detection in endoscopy," *Elsevier*, Accessed: Feb. 21, 2022. [Online]. Available: https://www.sciencedirect.com/science/article/pii/S0924424716301650

[25] K. Kim, K. Lee, W. Kim, K. Park, … T. K.-S. and A. A., and undefined 2009, "Polymer-based flexible tactile sensor up to 32× 32 arrays integrated with interconnection terminals," *Elsevier*, Accessed: Feb. 21, 2022. [Online]. Available: https://www.sciencedirect.com/science/article/pii/S092442470900377X

[26] K. Noda, K. Hoshino, K. Matsumoto, and I. Shimoyama, "A shear stress sensor for tactile sensing with the piezoresistive cantilever standing in elastic material," *Sensors and Actuators A: Physical*, vol. 127, no. 2, pp. 295–301, Mar. 2006, doi: 10.1016/J.SNA.2005.09.023.

[27] M. Tanimoto, F. Arai, T. Fukuda, … H. I.-… M. 98. I., and undefined 1998, "Micro force sensor for intravascular neurosurgery and in vivo experiment," *ieeexplore.ieee.org*, Accessed: May 08, 2022. [Online]. Available: https://ieeexplore.ieee.org/abstract/document/659809/?casa_token=1YDNgC3hsEcAAAAA:YcVnWHAusCab3dt1QDfQprH7vRDIIVasS-tXP5eemo6Nd_k0JYWb84cCppscbzr1Y4-zl3MOvUmq

[28] C. King, M. Culjat, … M. F.-I. T., and undefined 2008, "A multielement tactile feedback system for robot-assisted minimally invasive surgery," *ieeexplore.ieee.org*, Accessed: Feb. 21, 2022. [Online]. Available: https://ieeexplore.ieee.org/abstract/document/4674347/

[29] T. Kawasetsu, T. Horii, … H. I.-I. S., and undefined 2018, "Flexible tri-axis tactile sensor using spiral inductor and magnetorheological elastomer," *ieeexplore.ieee.org*, Accessed: Feb. 21, 2022. [Online]. Available: https://ieeexplore.ieee.org/abstract/document/8372916/

[30] H. Wang, D. Jones, G. de Boer, … J. K.-I. S., and undefined 2018, "Design and characterization of tri-axis soft inductive tactile sensors," *ieeexplore.ieee.org*, Accessed: Feb. 21, 2022. [Online]. Available: https://ieeexplore.ieee.org/abstract/document/8374831/

[31] L. Song, H. Zhu, Y. Zheng, … M. Z.-I. T., and undefined 2021, "Bionic compound eye-inspired high spatial and sensitive tactile sensor," *ieeexplore.ieee.org*, Accessed: Feb. 21, 2022. [Online]. Available: https://ieeexplore.ieee.org/abstract/document/9376688/

[32] A. Massaro, F. Spano, … A. L.-E.-I. T., and undefined 2011, "Design and characterization of a nanocomposite pressure sensor implemented in a tactile robotic system," *ieeexplore.ieee.org*, Accessed: Feb. 21, 2022. [Online]. Available: https://ieeexplore.ieee.org/abstract/document/5742700/

[33] J. J. Clark, "Magnetic Field Based Compliance Matching Sensor for High Resolution, High Compliance Tactile Sensing.," pp. 772–777, 1988, doi: 10.1109/robot.1988.12152.

[34] … W. N.-. 1991 I. I. C. on R. and undefined 1991, "Experimental results on Bayesian algorithms for interpreting compliant tactile sensing data," *ieeexplore.ieee.org*, Accessed: May 08, 2022. [Online]. Available: https://ieeexplore.ieee.org/abstract/document/131606/

[35] S. Youssefian, N. Rahbar, and E. Torres-Jara, “Contact behavior of soft spherical tactile sensors,” *IEEE Sensors Journal*, vol. 14, no. 5, pp. 1435–1442, 2014, doi: 10.1109/JSEN.2013.2296208.

[36] D. S. Chathuranga, Z. Wang, Y. Noh, T. Nanayakkara, and S. Hirai, “Disposable soft 3 axis force sensor for biomedical applications,” *Proceedings of the Annual International Conference of the IEEE Engineering in Medicine and Biology Society, EMBS*, vol. 2015-Novem, pp. 5521–5524, 2015, doi: 10.1109/EMBC.2015.7319642.

[37] L. Jamone, L. Natale, G. Metta, and G. Sandini, “Highly sensitive soft tactile sensors for an anthropomorphic robotic hand,” *IEEE Sensors Journal*, vol. 15, no. 8, pp. 4226–4233, 2015, doi: 10.1109/JSEN.2015.2417759.

[38] G. Chatzipirpiridis, P. Erne, O. Ergeneman, S. Pane, and B. J. Nelson, “A magnetic force sensor on a catheter tip for minimally invasive surgery,” *Proceedings of the Annual International Conference of the IEEE Engineering in Medicine and Biology Society, EMBS*, vol. 2015-Novem, pp. 7970–7973, 2015, doi: 10.1109/EMBC.2015.7320241.

[39] H. Wang *et al.*, “Design methodology for magnetic field-based soft tri-axis tactile sensors,” *Sensors (Switzerland)*, vol. 16, no. 9, 2016, doi: 10.3390/s16091356.

[40] D. S. Chathuranga, Z. Wang, Y. Noh, T. Nanayakkara, and S. Hirai, “Magnetic and Mechanical Modeling of a Soft Three-Axis Force Sensor,” *IEEE Sensors Journal*, vol. 16, no. 13, pp. 5298–5307, 2016, doi: 10.1109/JSEN.2016.2550605.

[41] T. P. Tomo *et al.*, “Design and characterization of a three-axis hall effect-based soft skin sensor,” *Sensors (Switzerland)*, vol. 16, no. 4, 2016, doi: 10.3390/s16040491.

[42] T. P. Tomo *et al.*, “A New Silicone Structure for uSkin - A Soft, Distributed, Digital 3-Axis Skin Sensor and Its Integration on the Humanoid Robot iCub,” *IEEE Robotics and Automation Letters*, vol. 3, no. 3, pp. 2584–2591, 2018, doi: 10.1109/LRA.2018.2812915.

[43] T. P. Tomo *et al.*, “Covering a Robot Fingertip with uSkin: A Soft Electronic Skin with Distributed 3-Axis Force Sensitive Elements for Robot Hands,” *IEEE Robotics and Automation Letters*, vol. 3, no. 1, pp. 124–131, 2018, doi: 10.1109/LRA.2017.2734965.

[44] N. J. Kumar, B. George, and M. Sivaprakasam, “A Sensor System to Assess the Ocular Digital Massage in an Ophthalmic Anaesthesia Training System,” *IEEE Sensors Journal*, vol. 19, no. 22, pp. 10812–10820, 2019, doi: 10.1109/JSEN.2019.2932195.

[45] A. Mohammadi, Y. Xu, Y. Tan, P. Choong, and D. Oetomo, “Magnetic-based soft tactile sensors with deformable continuous force transfer medium for resolving contact locations in robotic grasping and manipulation,” *Sensors (Switzerland)*, vol. 19, no. 22, pp. 1–14, 2019, doi: 10.3390/s19224925.

[46] D. Jones *et al.*, “Design and evaluation of magnetic hall effect tactile sensors for use in sensorized splints,” *Sensors (Switzerland)*, vol. 20, no. 4, pp. 1–13, 2020, doi: 10.3390/s20041123.

[47] C. Chi, X. Sun, N. Xue, T. Li, and C. Liu, “Recent progress in technologies for tactile sensors,” *Sensors (Switzerland)*, vol. 18, no. 4, 2018, doi: 10.3390/s18040948.

[48] Navaraj, William, and Ravinder Dahiya. "Fingerprint-enhanced capacitive-piezoelectric flexible sensing skin to discriminate static and dynamic tactile stimuli." *Advanced Intelligent Systems* 1.7 (2019): 1900051.

[49] Fastier-Wooller, Jarred W., et al. "Multimodal Fibrous Static and Dynamic Tactile Sensor." *ACS Applied Materials & Interfaces* 14.23 (2022): 27317-27327.

[50] Tolvanen, Jarkko, Jari Hannu, and Heli Jantunen. "Kirigami-inspired dual-parameter tactile sensor with ultrahigh sensitivity, multimodal and strain-insensitive features." *Flexible and Printed Electronics* 6.3 (2021): 034005